CHAPTER 3

RESULTS AND DISCUSSION

The results and discussion are separated into two parts: Zinc Oxide and Copper Oxide.

3.1 Synthesis of zinc oxide (ZnO) by a hydrothermal method with different alkaline base solution

In this part, zinc oxide compounds were synthesized by hydrothermal method. ZnO were fabricated on Zn metal plates as Zn source and substrate. Zn plates were cleaned with deionized water and absolute alcohol in an ultrasound bath, respectively. They were put in different kind of base at different pH of precursor's solution, heated the system in a laboratory electric oven. The final products were analyzed using XRD, SEM, TEM, and PL spectroscopy. The results and discussion are shown the morphologies, properties and compared the antibacterial activity of ZnO which synthesized in different kind of base (NaOH, LiOH).

3.1.1 Synthesis of ZnO with NaOH by a hydrothermal method

1) X-ray Diffraction (XRD)

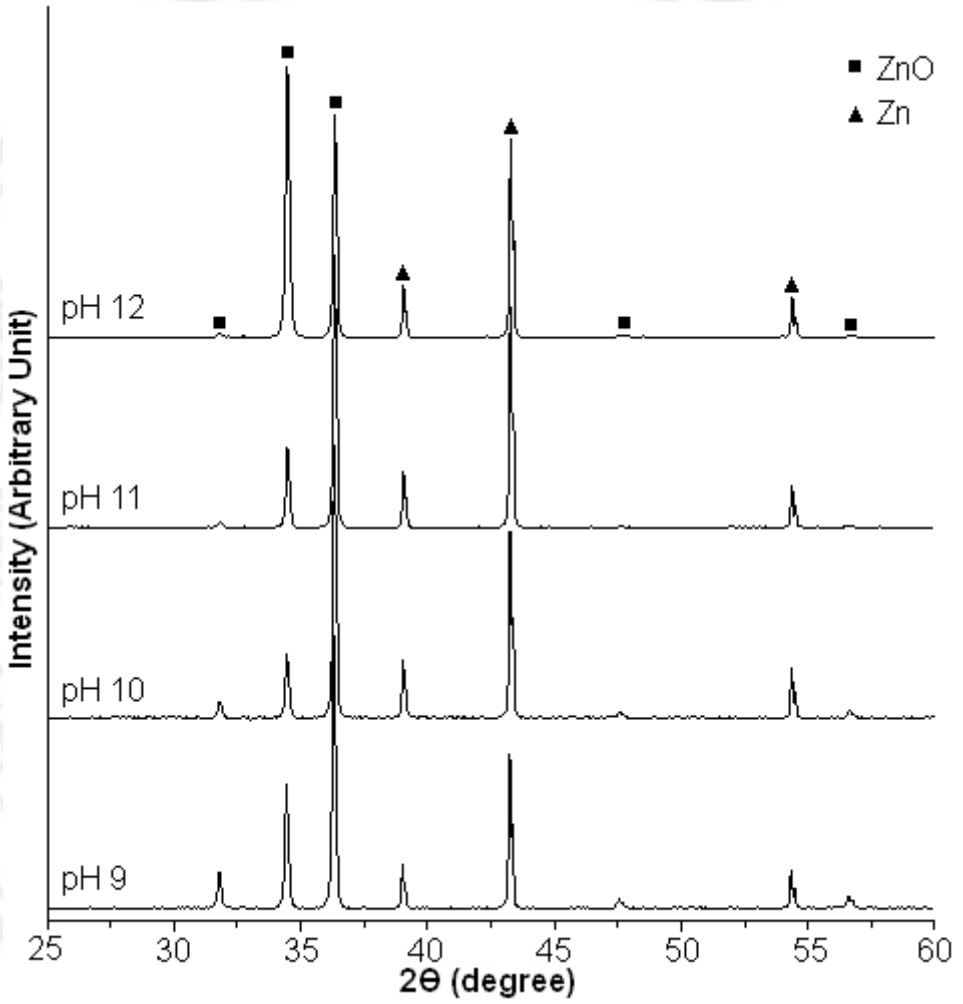

Figure 3.1 XRD pattern of as-synthesized ZnO samples at different pH synthesized by hydrothermal method.

The XRD pattern of the as-grown ZnO crystals on Zn foil synthesized by hydrothermal method at 120°C for 24 h at different pH of NaOH solutions are shown in Fig 3.1. Before hydrothermal treatment, all the diffraction peaks the XRD pattern can be indexed to pure hexagonal Zn structure. However, it was found that the products were wurtzite structured ZnO phase with comparing to JCPDS No. 36-1451[46] and other peaks except those marked with Zn with comparing to JCPDS No. 04-0831 [46] from the zinc substrate. It can see that diffraction peaks of as-synthesized ZnO samples are

sharper and stronger after increased pH of precursor solutions, which suggest that the ZnO sample should be well crystallized. As known as, the preferential orientation of synthetic 1D nanomaterial has relationship with the peak intensities of the as-prepared samples by compared with the standard diffraction pattern of bulk ZnO. It found that intensities of (0002) plane of as-synthesized ZnO sample show higher that (101) plane as a highest peak of bulk ZnO material, which may be related to the preferential orientation and alignment of the prepared ZnO crystals on Zn substrate. It implied that the preferential orientation ZnO grow along [0002] direction on the Zn substrate [47,48].

The degree of the c orientation of as-synthesized ZnO samples was explained by the relative texture coefficient (TC) [49-51]. The relative texture coefficient of the (002) peak was calculated using the formula,

$$TC002 = \frac{\left(I002 / I^{o}002\right)}{\left[I002 / I^{o}002 + I100 / I^{o}100\right]}$$

TC_{002} is the relative texture coefficient of the (002) over (100) diffraction peaks. I_{002} and I_{100} are the measured diffraction intensities of the (002) and (100) peaks, respectively. I^{o}_{002} and I^{o}_{100} are the corresponding values of the standard, measured from the randomly oriented powder. For random crystallographic orientation, the texture coefficient of ZnO is 0.5. Calculated TC_{002} is 0.74, which supports the preferential orientation as-prepared ZnO samples grow along [002] direction on the Zn substrate.

2) Scanning Electron Microscope (SEM)

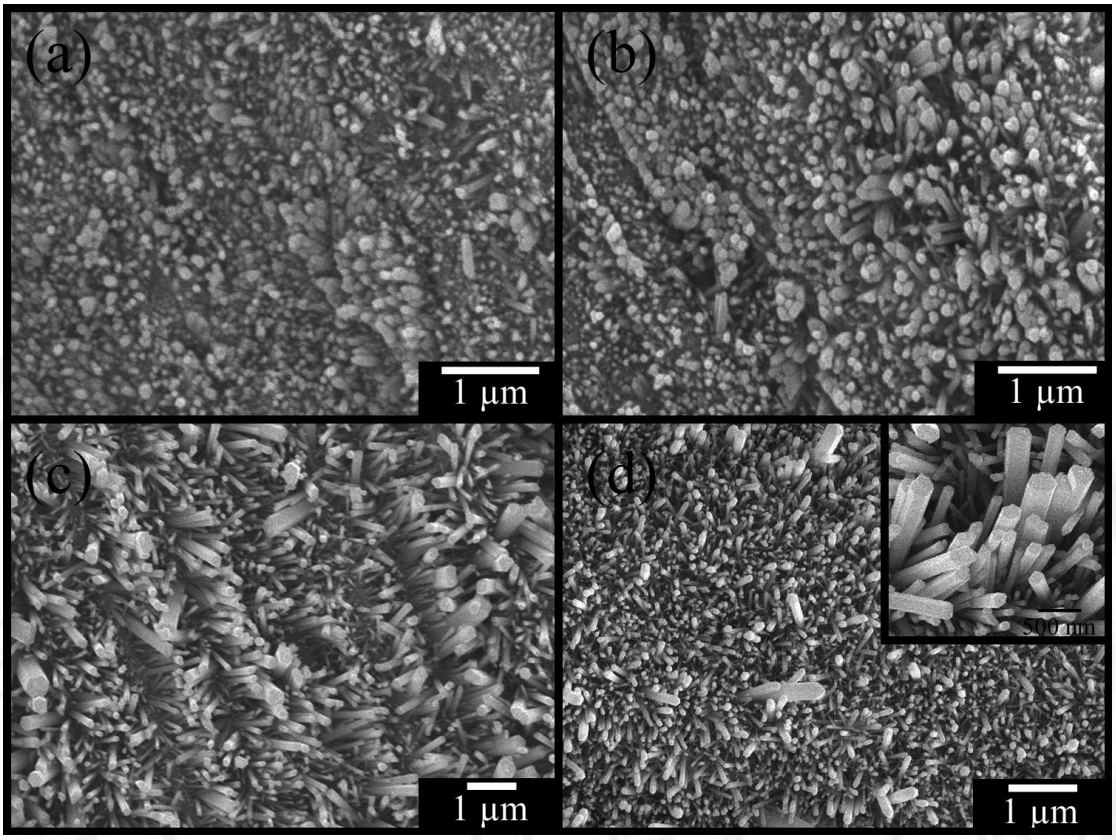

Figure 3.2 SEM images of as-synthesized ZnO synthesized at pH (a) 9, (b) 10, (c) 11 and (d) 12 synthesized by hydrothermal method.

The morphologies of as-synthesized ZnO samples grown on Zn foil were observed by SEM as shown in Fig. 3.2. It can be seen that the morphologies of products were evaluated from nanoparticles to nanorods, depending on the pH of solution. At low basicity (pH 9), the surface of the zinc substrate was uniformly covered ZnO nanoparticles. The ZnO nanoparticles begin growing into ZnO nanorods at pH 10. Increasing the pH of solution to 12, it can be clearly seen that the Zn substrate is densely and fully covered by ZnO nanorods with a diameter in the range of 100-500 nm and a length of 1 μm. The high-magnification of SEM image as inserted in Fig. 3.2d, it presented that the ZnO crystals exhibit obviously hexagonal prism shapes with angle between the two adjacent edges of an individual prism of 120^{o}. The prisms show well-resolved edges and corners with smooth surfaces.

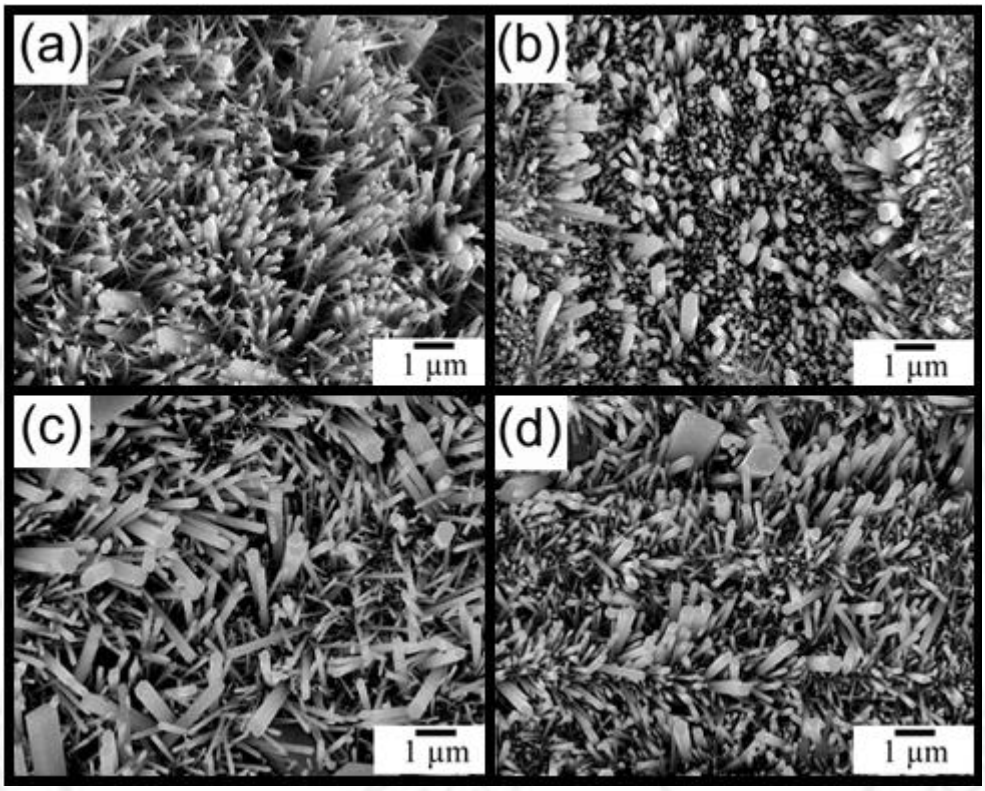

Figure 3.3 SEM images of as-synthesized ZnO samples at pH 12 with (a) 80°C, (b) 90°C, (c) 100°C and (d) 120°C synthesized by hydrothermal method.

The effect of temperature reactions were shown in Fig. 3.3. It can be seen that the sizes and morphologies of products were changed from nanopins (Fig. 3.3a) synthesized at 80°C to hexagonal prism nanorods (Fig. 3.3d) synthesized at 120°C. At 90 and 100°C, the morphologies of as-synthesized ZnO were the mix of nanopins and nanorods. So, we were concluded that the best condition to synthesize hexagonal prism ZnO nanorods.

3) Transmission Electron Microscope (TEM)

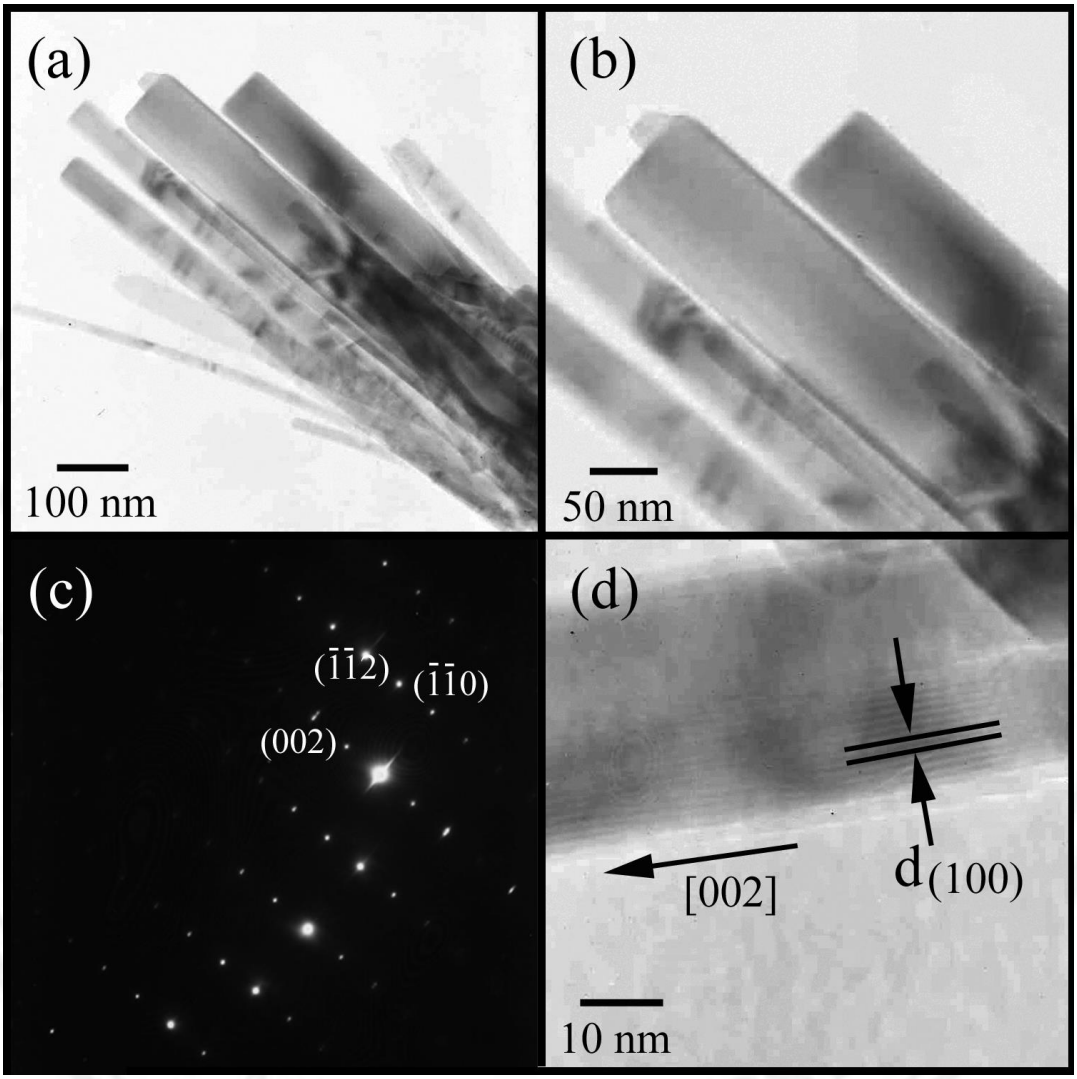

Figure 3.4 TEM image, SAED pattern and HRTEM image of hexagonal pyramids ZnO nanorods.

To more information of morphologies of the samples were investigated by TEM. The general TEM images, HRTEM image and SAED pattern of the as-synthesized ZnO sample at pH 12 are shown in Fig. 3.4. TEM images show rod-like ZnO nanostructures with a diameter range from 20 to 80 nm and lengths of several hundreds of nanometers. The corresponding selected-area electron diffraction (SAED) pattern was shown in the Fig. 3.4c. The SAED patterns from different positions of an individual nanorod indicated that ZnO nanorods were single-crystalline. It can be indexed to the hexagonal ZnO phase, which is in accordance with the XRD results. The HRTEM image shows

the inter-planar spacing of about 0.52 nm with corresponding to fringes of ZnO (1000) planes and confirms the single crystallinity with the preferential growth in the [0001] direction. SAED and HRTEM confirm that rod-likes ZnO nanostructures can grow along the [0001] direction [52,53]. The formation of hexagonal prisms shaped ZnO nanorods is attributed to the difference in the growth rate of the prominent of various crystal facets with low attachment energies during the growth of crystal. The surface energy of difference of hexagonal ZnO facets of (0001), (10-11), (10-10) planes are −2.8102, −2.1067 and −2.0013 kJ/mol, respectively [54-56]. Therefore, the growth velocities of the ZnO crystals in different planes are (0001) > (10-11) > (10-10). The (0001) plane disappears due to the most rapid growth rate leading to the pointed shape in an end of the *c*-axis. The growth rate of the {10-10} planes is small, and they remain to form the hexagonal prism ZnO nanorods [54-56].

4) Formation mechanism of ZnO

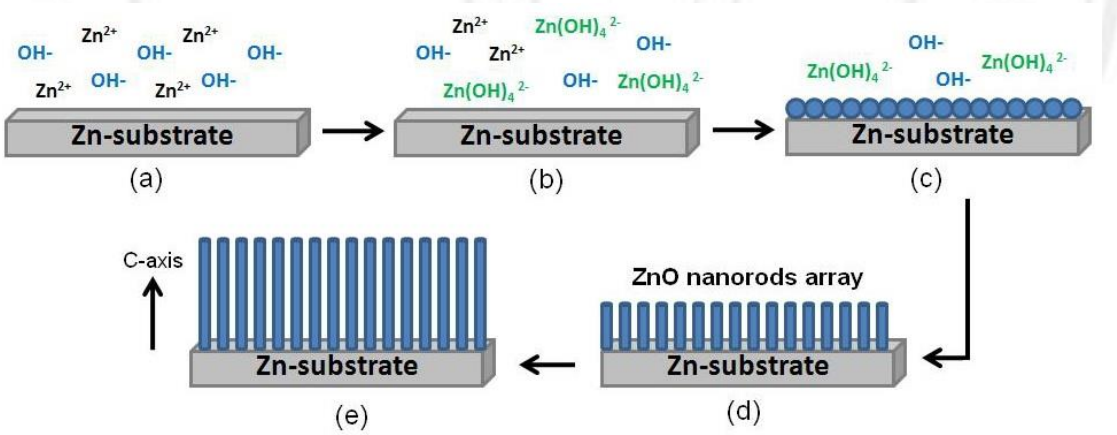

Figure 3.5 schematic diagram of possible growth mechanism of of hexagonal prism ZnO nanorods grow on Zn foil.

In general, the size and the morphology of the products depend on the competition between crystal nucleation and crystal growth, which are determined by the inherent crystal structure and the chemical potential in the precursor solution. Although the crystal growth habit is mainly determined by the intrinsic structure, it is also affected by the external conditions such as pH of the solution, saturation, temperature, etc. In this work, the condition of the pH of the solution as a factor is considered to play a key part

in the formation of hexagonal prism ZnO nanorods [57, 58]. Fig. 3.5 shows the schematic diagram of possible growth mechanism of hexagonal prism ZnO nanorods grow on Zn foil and simple explained in three basic steps. Firstly, the Zn^{2+} ions were dissolved from zinc foil as substrate, formation of growth unit $Zn(OH)_4^{2-}$ to create multiple nuclei on the zinc substrate and homoepitaxial growth of nuclei into hexagonal prism ZnO nanorods. Under hydrothermal condition, the Zn-foil substrate could be easily oxidized in reaction, and ZnO nanoparticles may be generated to form ZnO thin layer on the Zn-foil substrate in reaction. Consequently, ZnO nuclei produced in solution can aggregate to form small particles. These particles may serve as crystal seeds for the continuous epitaxial growth of ZnO nuclei into hexagonal prism ZnO nanorods structures on the surface of Zn-foils. With the pH increase continuing, a large amount of ZnO nuclei produced in the solution, resulting in a very high supersaturated solution, which favors the formation of hexagonal prism ZnO nanorods. Hence, the special growth behavior formation of hexagonal prism ZnO nanorods on Zn foil substrates in the present route is attributed to the highly pH in basicity [38,59].

5) Photoluminescent (PL) Spectroscopy

In terms of the optical properties of 1D ZnO nanostructures, two emission bands are commonly found in the photoluminescence (PL) spectrum of ZnO nanorods. The UV emission occurs by the transition of excitons, while the visible emission occurs due to surface defects of thecrystal. Various rationalizations have been suggested to explain the change in PL of 1D ZnO nanostructures. The intensity of UV emission has its maximum value when the 1D ZnO nanostructures have an orientation along the c-axis, and this increases as the crystal size increases. Meanwhile, surface defects, interstitial defects, and the absorption of impurities onto the surface of the nanorods are known to result in various emissions in the visible range. For example, green emission is known to occur by the recombination of a photogenerated hole with an electron occupying intrinsic defect, such as a single ionized oxygen vacancy(V_{O+}) , an oxygen antisite (O_{Zn}), or a zinc vacancy (V_{Zn}). Regarding the origin of yellow emission, opinions are divided into the zinc interstitial(Zn_i) and oxygen interstitial defects (O_i^-). On the

otherhand, yellow–green emission is reported to decline with the desorption of the OH groups on the surface of the ZnO [60,61].

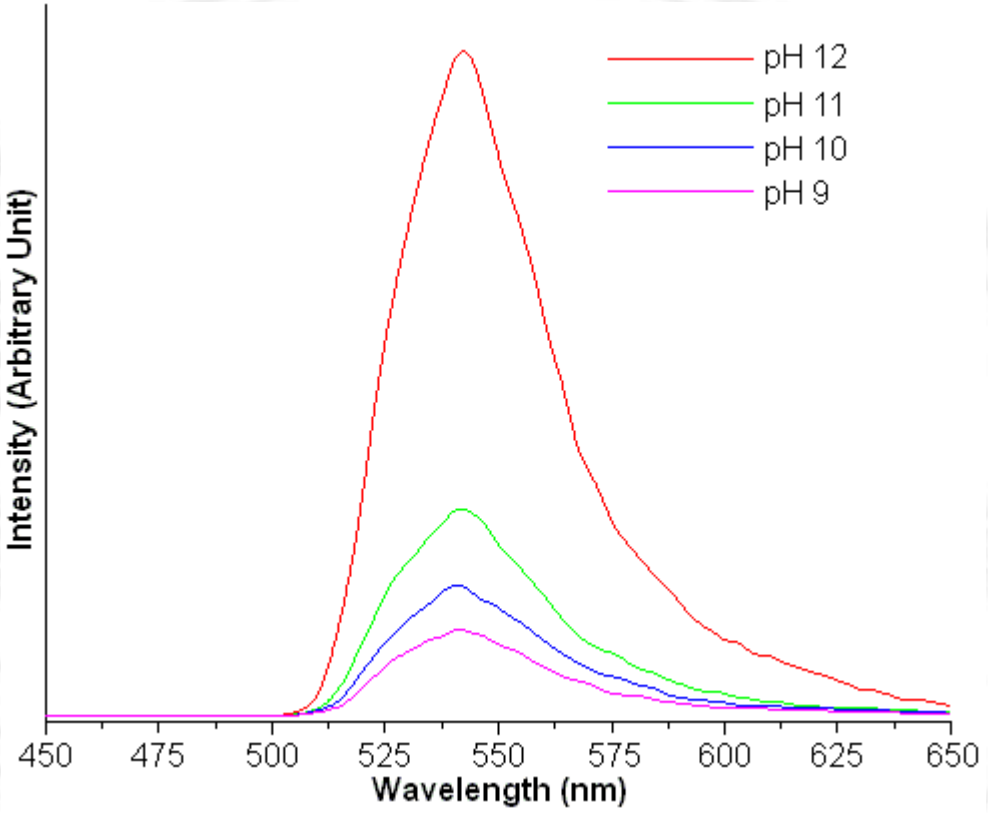

Figure 3.6 PL spectra of as-synthesized ZnO samples at difference pH synthesized by hydrothermal method.

The room-temperature PL spectra of the hexagonal prisms shaped ZnO were measured using excitation wavelength of 215 nm as shown in Fig. 3.6. They show a same emission broad band at 510-640 nm and a strong band at 543 nm. The green-yellow emission results from the recombination of electrons with holes trapped in singly ionized oxygen vacancies [62-64]. These emissions may find use in optoelectronics applications.

3.1.2 Synthesis of ZnO with LiOH by a hydrothermal method

1) X-ray Diffraction (XRD)

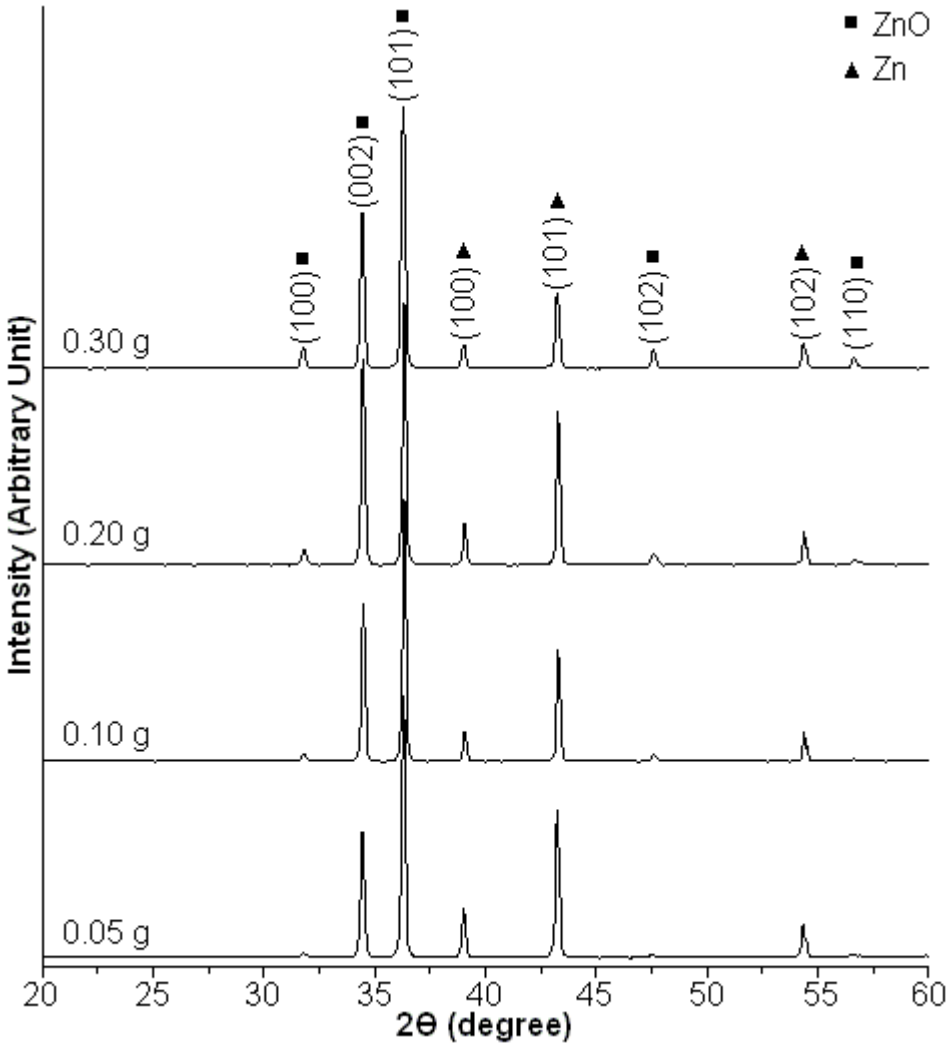

Figure 3.7 XRD pattern of as-synthesized ZnO samples at difference weights of LiOH.

The crystal structure and phase of the as-synthesized ZnO grow on Zn foils were investigated by XRD as shown in Fig. 3.7. They can be indexed to (100), (002), (101), (102) and (110) planes at $2\theta = 31.77$, 34.45, 36.30, 47.53 and 56.06 of wurtzite hexagonal ZnO structure with comparison to with JCPDS No. 36-1451 [46] and (002), (100) (101) and (102) planes at $2\theta = 36.30$, 39.03, 43.26 and 54.33 of hexagonal Zn structure with comparison to with JCPDS No. 04-0831 [46]. The sharpness of the peaks

implies high crystallinity of the as-prepared sample. It is worth noting that the strong diffraction peaks of relative intensity come from (101) and (002) of wurtzite hexagonal ZnO phase, suggesting that the ZnO nanorods would have a preferential growth direction along the [101] and [002] directions [65].

2) Scanning Electron Microscope (SEM)

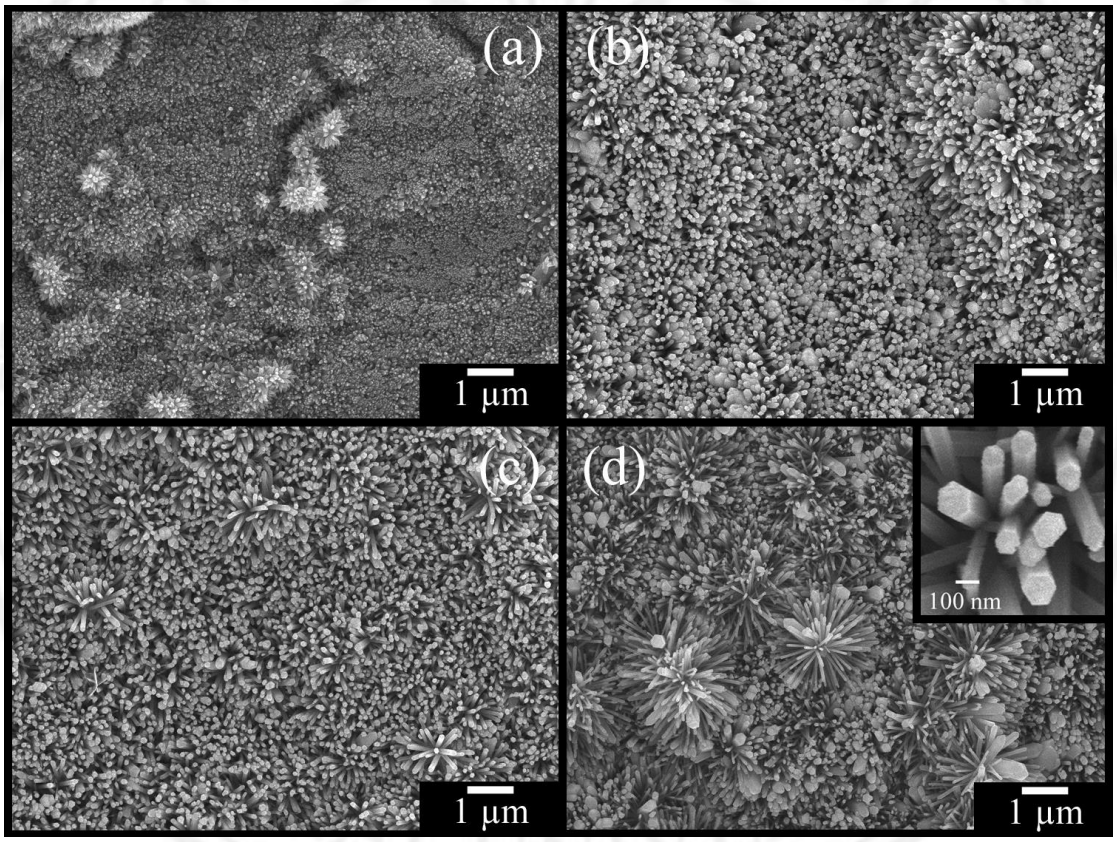

Figure 3.8 SEM images of ZnO samples using 0.10 g of LiOH synthesized by hydrothermal method.at 120^{o}C for (a) 1, (b) 6, (c) 18 and (d) 24 hrs.

The morphologies of as-synthesized ZnO samples grow on Zn foil were observed by SEM. Figure 3.8 shows the as-synthesized ZnO samples grow on Zn foil as substrate synthesized by hydrothermal using 0.1 g LiOH at 200^{o}C for different times. It can be clearly seen from Fig. 3.8a that ZnO nanorods arrays uniformly covered the entire surface of the zinc substrate. The ZnO nanorods become highly oriented and dense ZnO hexagonal nanorods in large-scale uniform arrays with diameters of 50 nm are aligned on the Zn foil surface when increased hydrothermally reaction time to 6 h. To prolong

reaction time to 24 h, it revealed that ZnO flower-like composed of a hexagonal prism shapes grow form flower-like ZnO core on ZnO hexagonal nanorods arrays. The individual hexagonal prism ZnO has a diameter in the range of 100 nm and a length of 1-2 μm. At high magnification SEM images as inserted in Fig. 3.8d, it present that the ZnO crystals exhibit obviously hexagonal prism shapes with angle between the two adjacent edges of an individual prism of 120^{o}. As known as, the elongated form of these crystals is the result of growth anisotropy between different crystal faces. The hexagonally prismatic shape of ZnO crystals suggests two principal types of face-specific growth. A axial growth is normal to the (0001) lattice planes and directed along the c-axis of symmetry, and equatorial growth, which is normal to the (1010) planes and directed radially from the c-axis. It suggest that the growth of the individual ZnO hexagonal prism shapes is along the six symmetric directions of ±[10-10], ± [1-100] and ± [01-10] with the typical growth along [0001] direction suppressed, which directly leads to the formation of hexagonal prism ZnO nanorods [52-56].

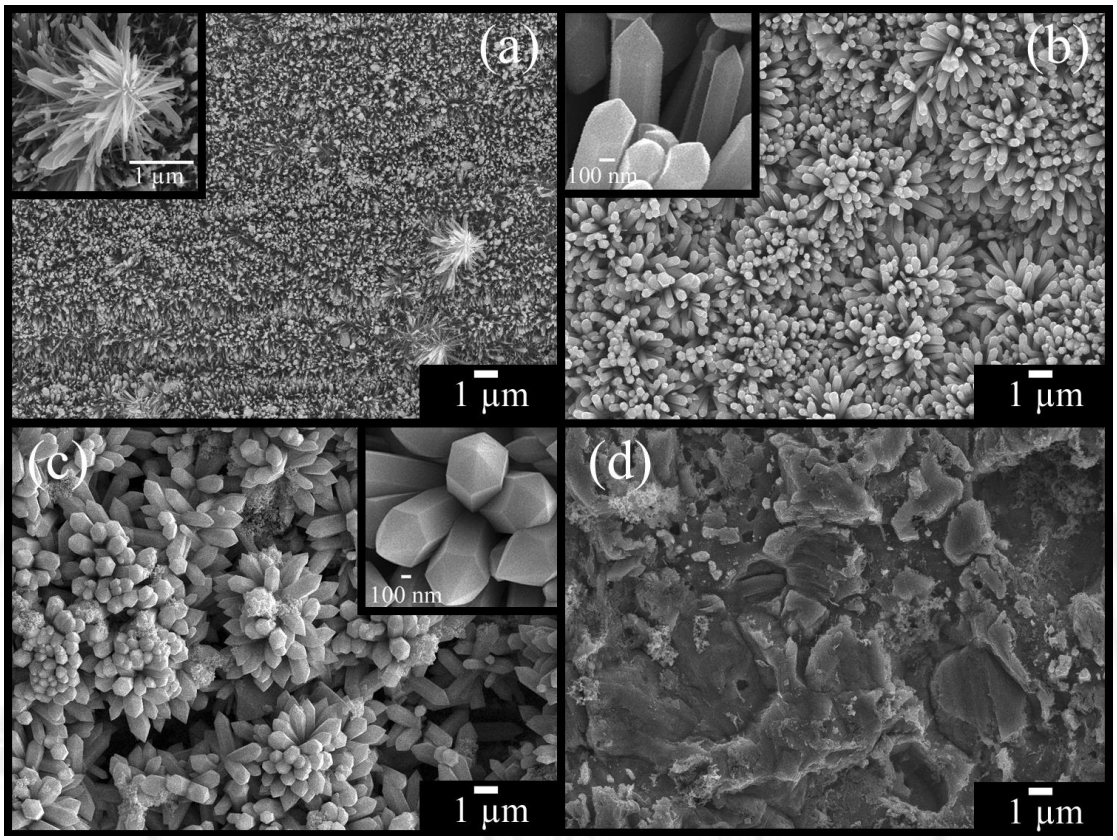

Figure 3.9 SEM images of XRD pattern of as-synthesized ZnO samples synthesized by hydrothermal method.at 120°C for 24 h using a) 0.05, (b) 0.20, (c) 0.30 and (d) 0.40 g of LiOH.

Figure 3.9 shows the SEM image of effect of weight of LiOH on morphologies of as-synthesized ZnO samples grow on Zn foil prepared by hydrothermal at 120^{o}C for 24 h. It can be clearly seen that the substrate is densely covered by hexagonal prism ZnO nanorods using 0.05 g LiOH. The ZnO nanorod arrays have length of about 1 μm and diameters of 200 nm on average. In another region of the Zn-foil, flower-like ZnO nanorods composed of several hexagonal prism shapes grow on the ZnO hexagonal nanorods arrays. Using 0.20 and 0.30 g of LiOH, they found that flower-like ZnO microstructures were fully and cover grow on the Zn foil. The top-view and the side-view of the enlarge top tips of the flower-like ZnO microstructures are inserted in Fig. 3.9b and 3.9c. They reveal that an individual ZnO microstructure exhibits an obvious hexagonal prism shape and has a hexagonal pyramid-like sharp tip showing well-defined crystallographic facets. However, the irregular and agglomerate ZnO was covered on the surface of the zinc substrate by hydrothermally treated at 200^{o}C for 24 h using 0.40 g of LiOH. In general, ZnO crystal is a polar crystal, and O^{2-} is in hexagonal closest packing (HCP) and each Zn^{2+} lies within a tetrahedral group of four oxygen ions. Zinc n and oxygen atoms are arranged alternatively along the c-axis. The occupancy of four of the eight tetrahedral sites of HCP arrays controls the structure. The inherent asymmetry along the c-axis results in the anisotropic growth of ZnO crystallites. The formation of hexagonal prism shaped ZnO crystals in the present study is suggested to be attributed to the difference in the growth rate of the various crystal facets. It is acceptable that (0001) is not a stable facet under hydrothermal conditions, and the hydrothermal growth rate of different planes is as follows: (0001)>(10-11)>(10-10). As we know, the more rapid the growth rate, the quicker the disappearance of the plane. Therefore, the relative growth rate of these crystal faces will determine the aspect ratio and the final shape of the ZnO nanostructures. The (0001) plane disappears due to the most rapid growth rate leading to the pointed shape in an end of the c-axis. The growth rate of the (10-10) planes is small, and they remain to form the hexagonal prisms, while the (10-11) planes mediate and remain to form hexagonal pyramid-like tips [38].

3) Transmission Electron Microscope (TEM)

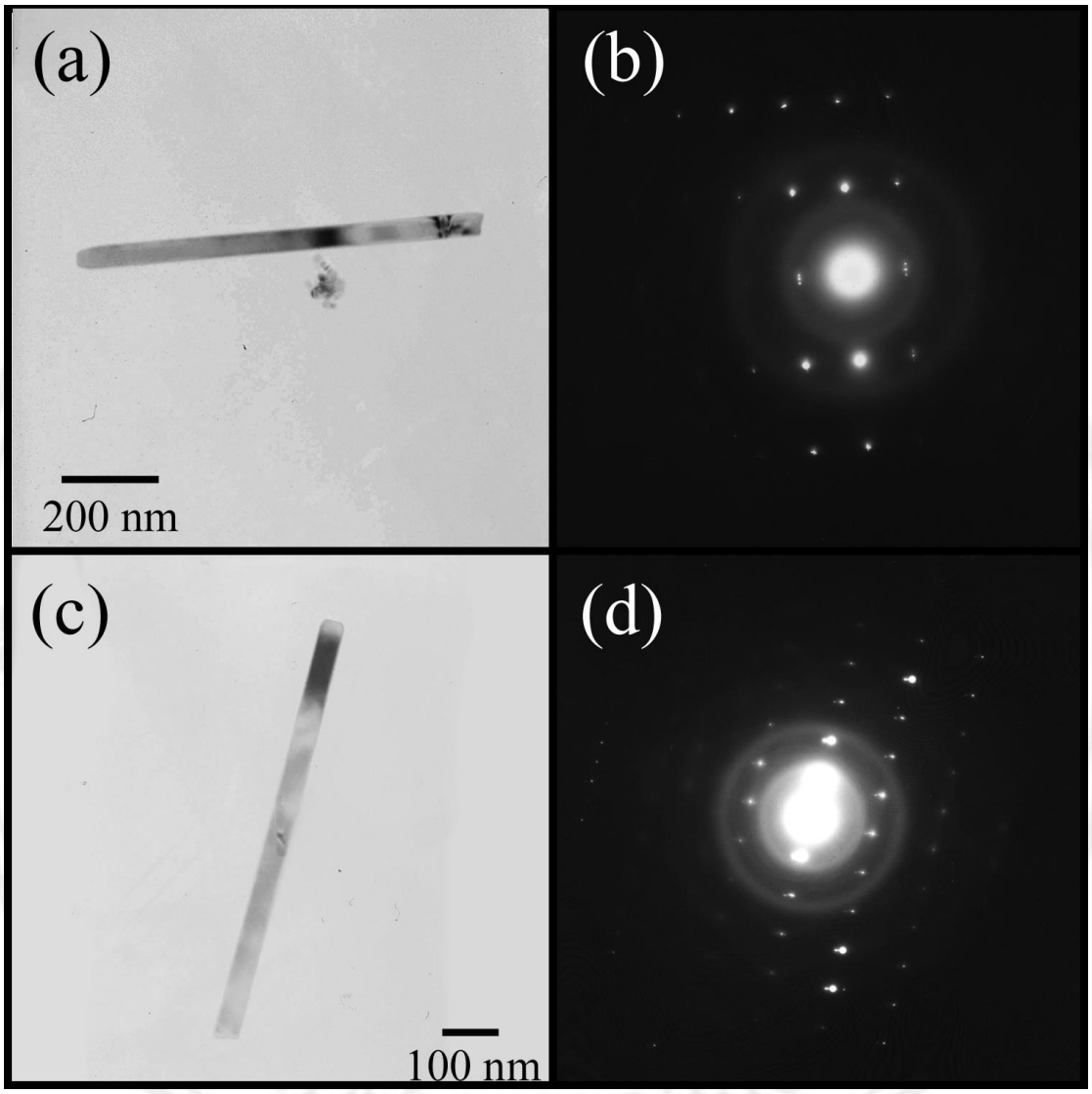

Figure 3.10 TEM image and SAED pattern and HRTEM image of hexagonal pyramids ZnO nanorods.

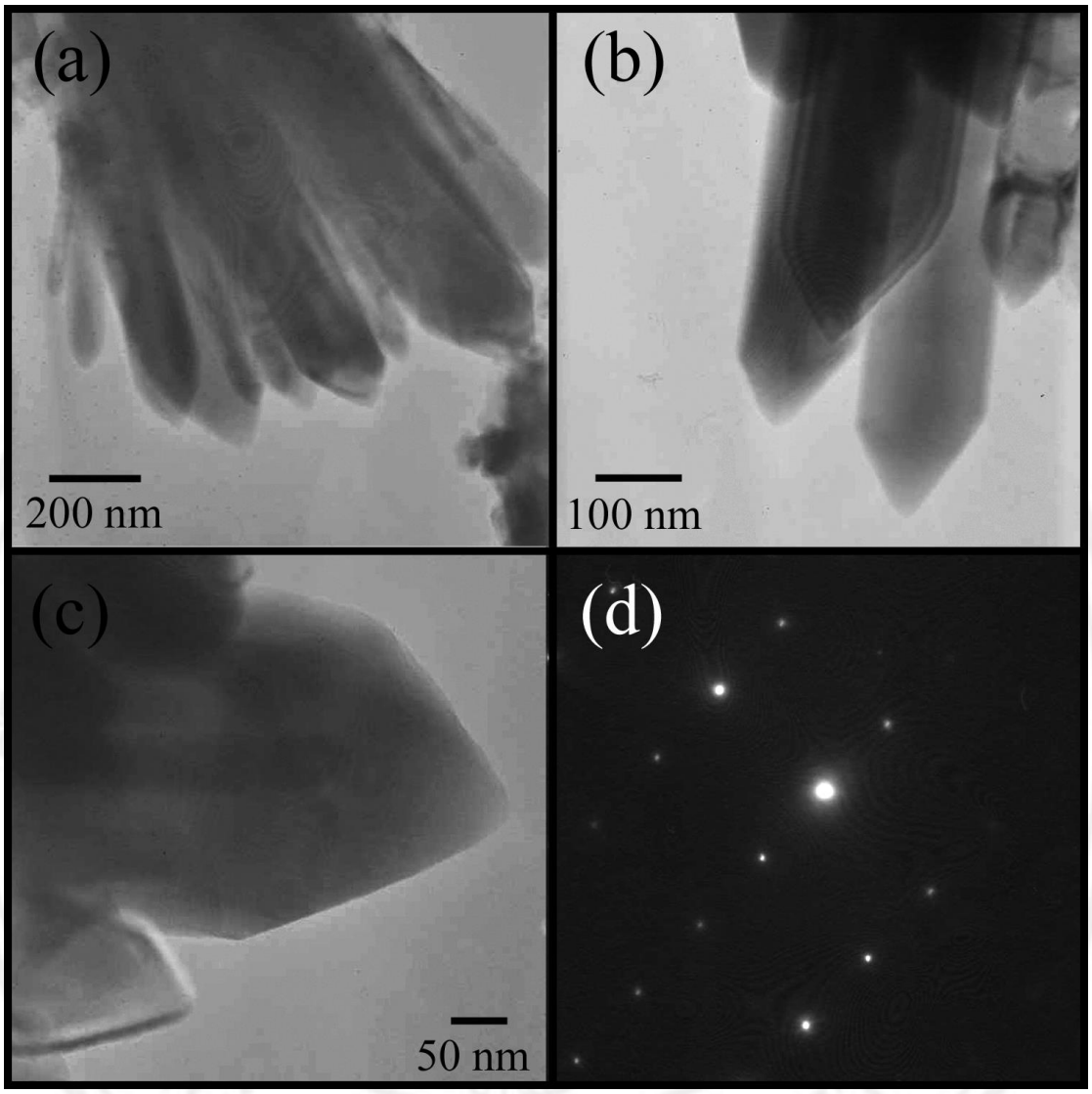

Figure 3.11 TEM image and SAED pattern and HRTEM image of hexagonal pyramids ZnO nanorods.

Further structural characterization of the flower-like hexagonal prisms and hexagonal pyramids ZnO microstructures arrays grown on the zinc foil substrate was performed by TEM. Fig. 3.10 shows the TEM images and SAED patterns of flower-like ZnO hexagonal prisms nanostructures Figs. 3.10a and 3.10c show the TEM image of a nanorod broken form flower-like ZnO hexagonal prisms with a diameter of 50 nm and length of 800 nm. It can be seen that the surface of ZnO nanorods is a very smooth. SAED pattern of single ZnO nanorod is a spot pattern, suggesting that ZnO nanorods are single-crystalline in structure. They can be identified as the [01−10] zone axis

projection of the ZnO reciprocal lattice. They indicate that the ZnO nanorods grow preferentially along the [0001] direction [52-56]. To understand the observed behaviors of ZnO, it is necessary to study its growth mechanism. As a wurtzite-structured metal oxide, zinc oxide belongs to the *P*63*mc* space group and has a highly anisotropic structure along the *c*-axis. The (0001) plane (terminated with zinc) of ZnO has the maximum surface energy, while the (000−1) plane (terminated with oxygen) has the minimum surface energy. As a result, the growth along the [0001] direction has a faster rate than that along other directions and is much more favorable. Thus, ZnO nanorods are easily formed.

Fig. 3.11a displays a typical TEM image of hexagonal pyramids ZnO microstructures broken form flower-like ZnO hexagonal pyramids. The flower-like ZnO microstructure is built from the hexagonal pyramids ZnO shape. The magnified tip structure of the petal was shown in Fig. 3.11b, presents that it is an assembly of several well-aligned nanoneedles. The approximate length and diameter of hexagonal pyramids are 600 and 80 nm. They exhibit a uniform diameter along their entire length. The tip of ZnO nanorod as shown in Fig. 3.11c shows a pyramid morphologies which is same SEM result. Fig. 3.11d shows the spot SAED pattern of single hexagonal pyramids ZnO nanorods, which indicates that the ZnO nanorod is single-crystalline in structure, according to the features of the diffraction pattern. It indicates that the hexagonal pyramids ZnO nanorod growth occurs preferentially along the [0001] direction.

4) Formation mechanism of ZnO

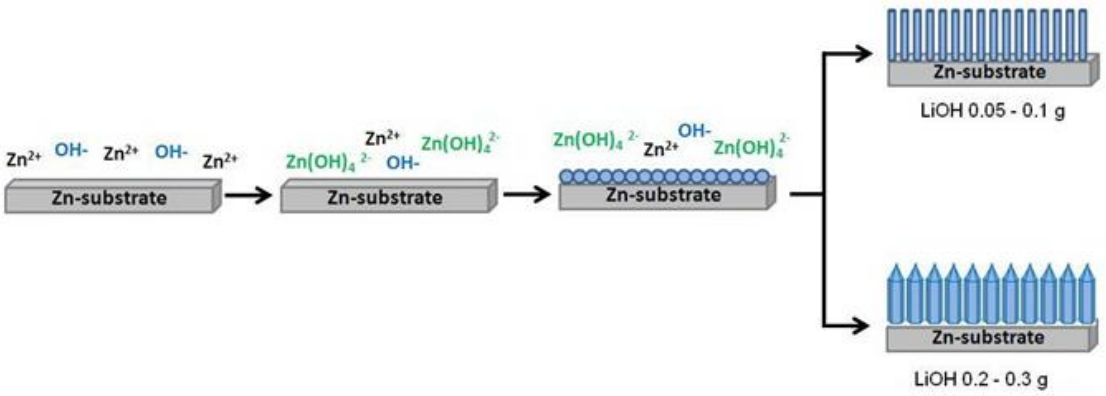

Figure 3.12 schematic diagram of possible growth mechanism of hexagonal prisms and hexagonal pyramids ZnO microstructures grow on Zn foil.

Figure 3.12 shows the schematic diagram of possible growth mechanism of hexagonal prisms and hexagonal pyramids ZnO nanostructures grow on Zn foil. In a typical solution based synthetic approach, $[Zn(OH)_4]^{2-}$ serve as a basic growth unit for the fabrication of ZnO nanoforms. Therefore in the present hydrothermal condition, Zn2+ ions are produced from the Zn foils which then react with the OH^- ions form LiOH to produce $[Zn(OH)_4]^{2-}$. These $[Zn(OH)_4]^{2-}$ ions then decompose to produce ZnO molecular species, forming a ZnO seed on the Zn Foil. These ZnO seeds grew to form a hexagonal planar nucleus. The hexagonal wurtzite ZnO with polar structure can be described as a hexagonal close packing of oxygen and zinc atoms in point group 3m and space group P63mc with zinc atoms in tetrahedral sites. Thus, the crystal habits of wurtzite ZnO exhibit well defined crystallographic faces i.e., basal (001) and non polar low symmetry (100) faces. In the case of wurtzite ZnO crystals as polar crystal, the each Zn^{2+} lies within a tetrahedral group of four oxygen ions. The Zn and oxygen atoms are arranged alternatively along the *c*-axis so that the top surface is Zn-terminated (0001) and the bottom surface is O^{2-}-terminated (000−1). The inherent asymmetry along the *c*-axis leads to the anisotropic growth of 1-D ZnO crystallites. The formation of hexagonal prism shaped ZnO crystals in the present study is suggested to be attributed to the difference in the growth rate of the various crystal facets. It is acceptable that the hydrothermal growth rate of different planes is as follows: (0001) > (10−1−1) > (10−10). As we know, the more rapid the growth rate, the quicker the disappearance of

the plane. Therefore, the relative growth rate of these crystal faces will determine the aspect ratio and the final shape of the ZnO nanostructures. The (0001) plane disappears due to the most rapid growth rate leading to the pointed shape at the end of the *c* axis. The growth rate of the (10−10) planes is small and they remain to form the hexagonal prisms at low pH. However, the polar (001) surface is metastable in nature and is subjected to etching at high pH conditions. It is possible that the Zn atoms of the (001) metastable polar surface react with the OH^- ions, forming the hydroxide species. The side facets of hexagonal prisms on six symmetric directions of ±[10-10], ± [1-100] and ± [01-10] were etched and (10−11) planes remain to form hexagonal pyramid-like tips. At the same time, the one-dimensional growth continues to give rise to the hexagonal pyramid ZnO nanostructures [52-56].

5) Photoluminescent (PL) Spectroscopy

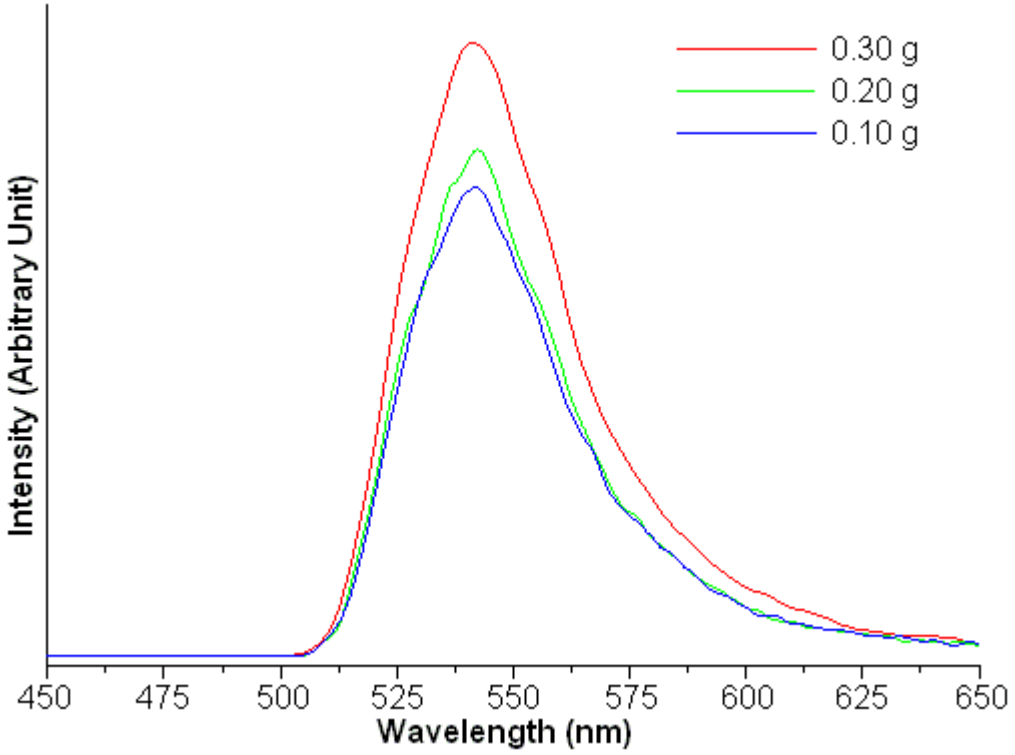

Figure 3.13 PL spectra of as-synthesized ZnO samples at difference weights of LiOH synthesized by hydrothermal method.

The photoluminescence (PL) is used to study the optical properties of ZnO as a photonic material as shown in Fig. 3.13 using the excitation wavelength of 215 nm at room temperature. PL spectra of ZnO products show the emission broad band at 505-625 nm in visible light. They have a same strong green emission band centered at 543 nm which related a defect in ZnO structure. The green emission is usually considered to be related to various intrinsic defects produced during ZnO preparation, but the exact mechanism is still under controversy. The presence of oxygen vacancies (V_O), zinc vacancies (V_{Zn}), interstitial zinc (Zn^i) and antisite defects (O_{Zn}) has been attributed to correspond to the yellow-green emission of ZnO [60-64]. There have been many proposed models that explain the emission from defect structures in ZnO crystals. It is generally believed that the yellow-green emission corresponds to the singly ionized oxygen vacancy in ZnO and results from the recombination of a photo-generated hole with the single ionized charge state of this defect [60-64].

3.1.3 Comparing the antibacterial activity of ZnO, synthesized with different kind of base by a hydrothermal method

1) X-ray Diffraction (XRD)

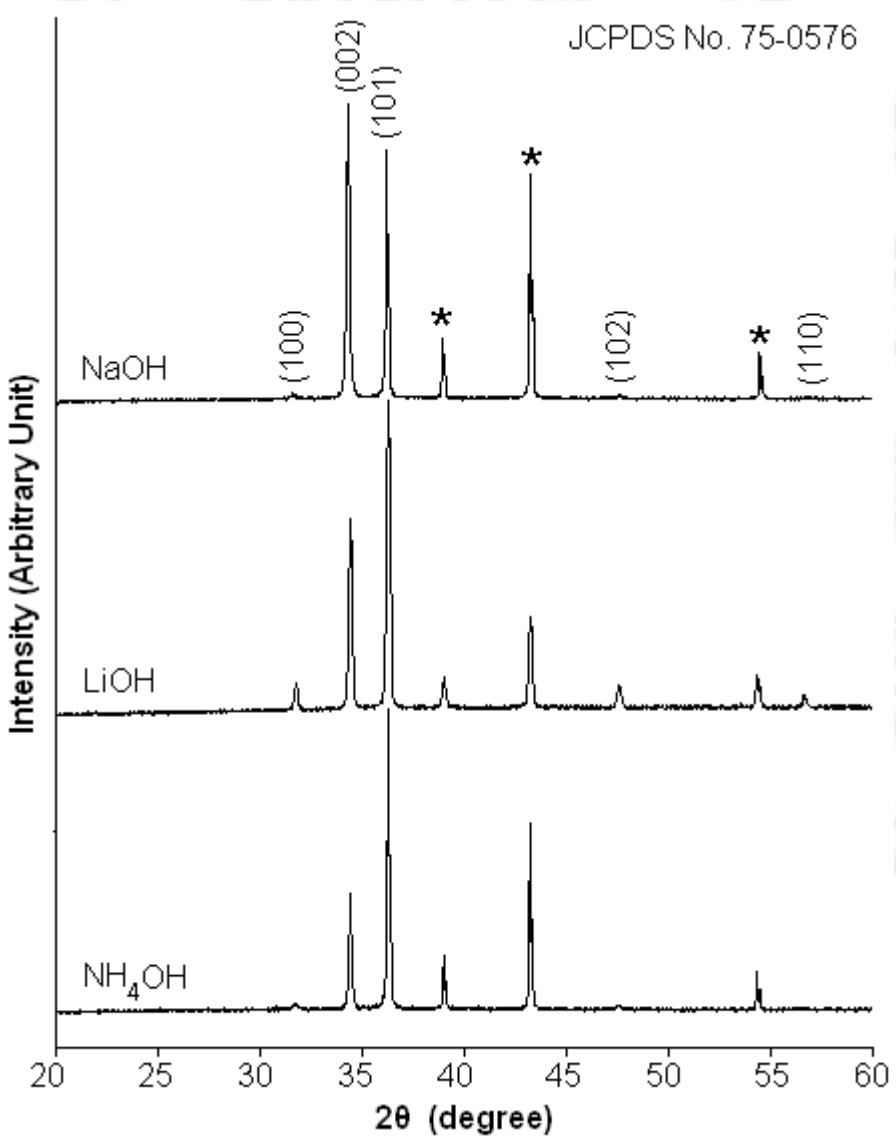

Figure 3.14 XRD patterns of ZnO synthesized in NaOH, LiOH and NH_4OH alkaline precursor solutions.

The XRD patterns (Fig. 3.14) of ZnO films synthesized in NaOH, LiOH and NH_4OH solutions on Zn substrates were very sharp, implying the existence of products with good crystalline degree. All diffraction patterns can be indexed to be hexagonal wurtzite structure, compared to JCPDS No. 75-0576 [46], including additional peaks marked with asterisks indexed to be Zn substrates compared to JCPDS No. 04-0831 [46]. No characteristic peaks of other impurities were detected. The XRD pattern of ZnO product synthesized in NaOH solution shows the highest diffraction peak at 34.45°, which illustrates the texture effect of the highly preferential orientation of ZnO product along the c-axis perpendicular to the substrate [65]. For the synthesis in LiOH and NH_4OH solutions, the (101) peaks were at the highest. It should be noted that strong diffraction peaks with the highest relative intensities diffracted from the (002) and (101) planes of wurtzite hexagonal ZnO phase, suggesting that the 1D ZnO would have preferential growth along the [002] and [101] directions [65], respectively.

2) Raman Spectroscopy

Vibrational properties of as-grown hexagonal shaped ZnO were investigated by Raman spectroscopic technique. In this research, ZnO was wurtzite hexagonal phase belonging to the space group of C_{6v}^4, having two formula units per primitive cell and all atoms occupy the sites of symmetry C_{3v}. According to the group theory, single crystalline ZnO has eight sets of optical phonon modes at the Γ point of the Brillouin zone ($2A_1 + 2B_1 + 2E_1 + 2E_2$). Among these optical phonon modes, the A_1 and E_1 modes are polar in nature and therefore split into two as transverse optical (TO) and longitudinal optical (LO) phonons. The remaining six optical modes, $A_1 + 2B_1 + E_1 + 2E_2$, can be detected for the first-order Raman scattering. The A_1 and E_1 modes are both Raman and infrared (IR) active, but the two E_2 modes are only Raman active. The two B_1 modes are neither Raman nor IR active (silent) modes [66].

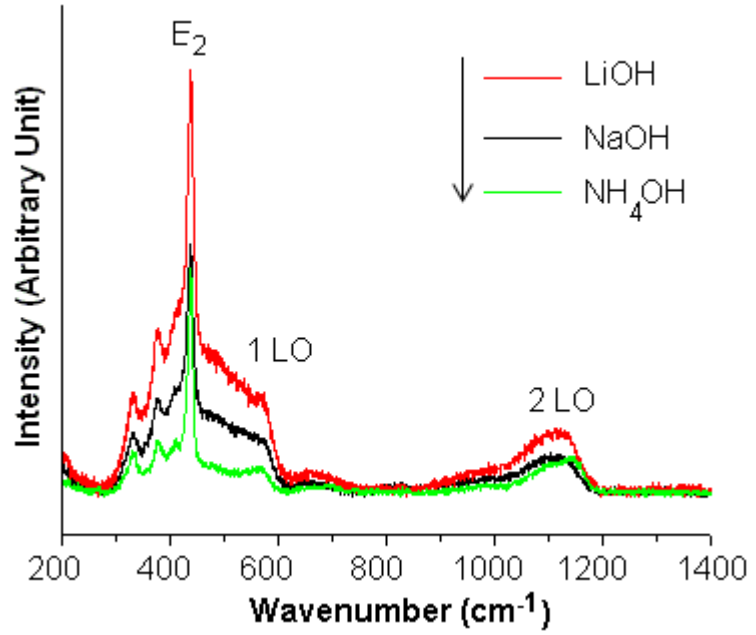

Figure 3.15 Raman spectra of ZnO synthesized in NaOH, LiOH and NH_4OH alkaline precursor solutions.

Figure 3.15 shows Raman spectra of the as-grown hexagonal structured ZnO on Zn substrates synthesized in NaOH, LiOH and NH_4OH alkaline solutions. The strong peaks at 437 cm^{-1} are due to the Raman active E_2 optical phonon mode (LO) of the ZnO products, confirming that they are the wurtzite hexagonal crystal structure – in accordance with the above XRD analysis [66,67]. The peaks at 581 cm^{-1} assigned to A_1(LO) mode were also detected. They could be due to the misalignment of rods or the formation of defects such as zinc interstitials and oxygen vacancies [66]. The second-order vibration modes were detected at 1110 cm^{-1} [67].

3) Scanning Electron Microscope (SEM)

The low magnification SEM images and their inserts as high magnification images (Fig. 3.16) show the different morphologies of ZnO films synthesized on Zn substrates in NaOH, LiOH and NH_4OH alkaline solutions. In this research, ZnO nanorods with average size of 100 nm in diameter and 500 nm in length, pencil-like ZnO with about 300 nm diameter and >800 nm long, and 3D star-like ZnO with the average size of each

pod of 200 nm in diameter and 1 μm in length were synthesized in the NaOH, LiOH and NH_4OH alkaline solutions, respectively.

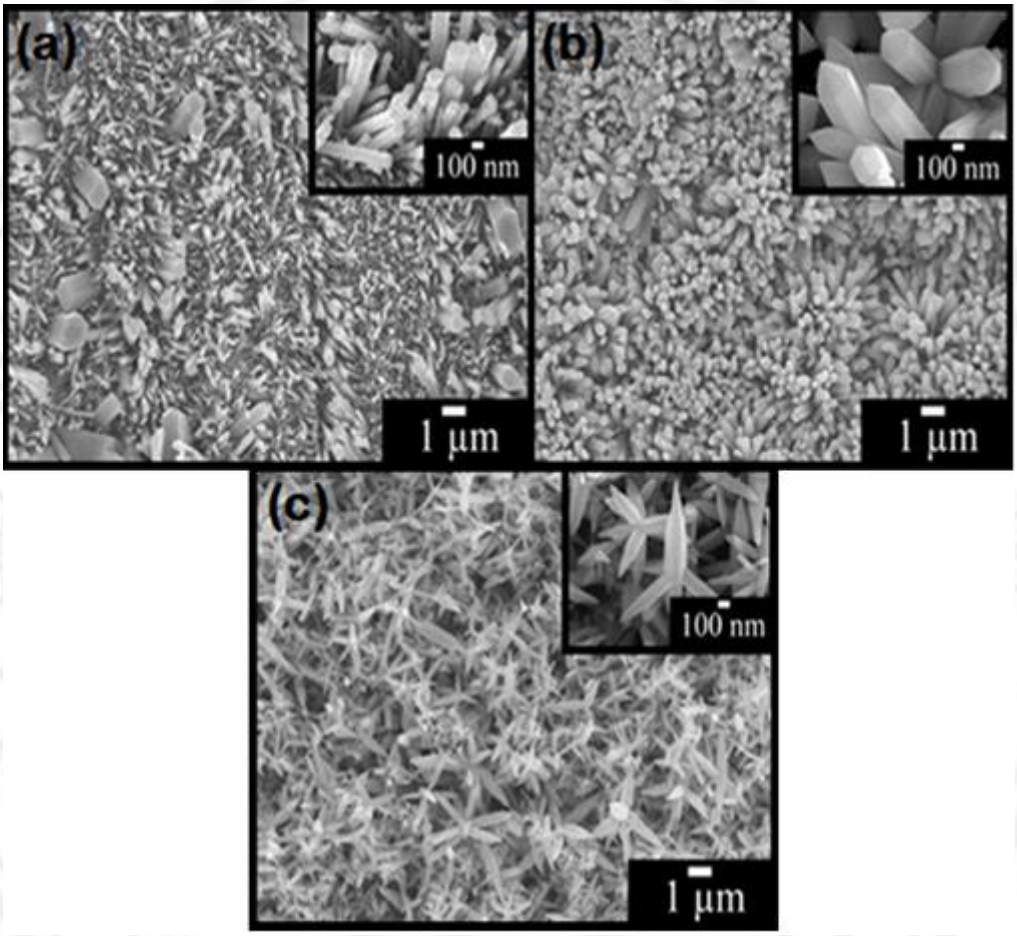

Figure 3.16 SEM images of ZnO synthesized in (a) NaOH, (b) LiOH and (c) NH_4OH alkaline precursor solutions.

4) Transmission electron microscope (TEM)

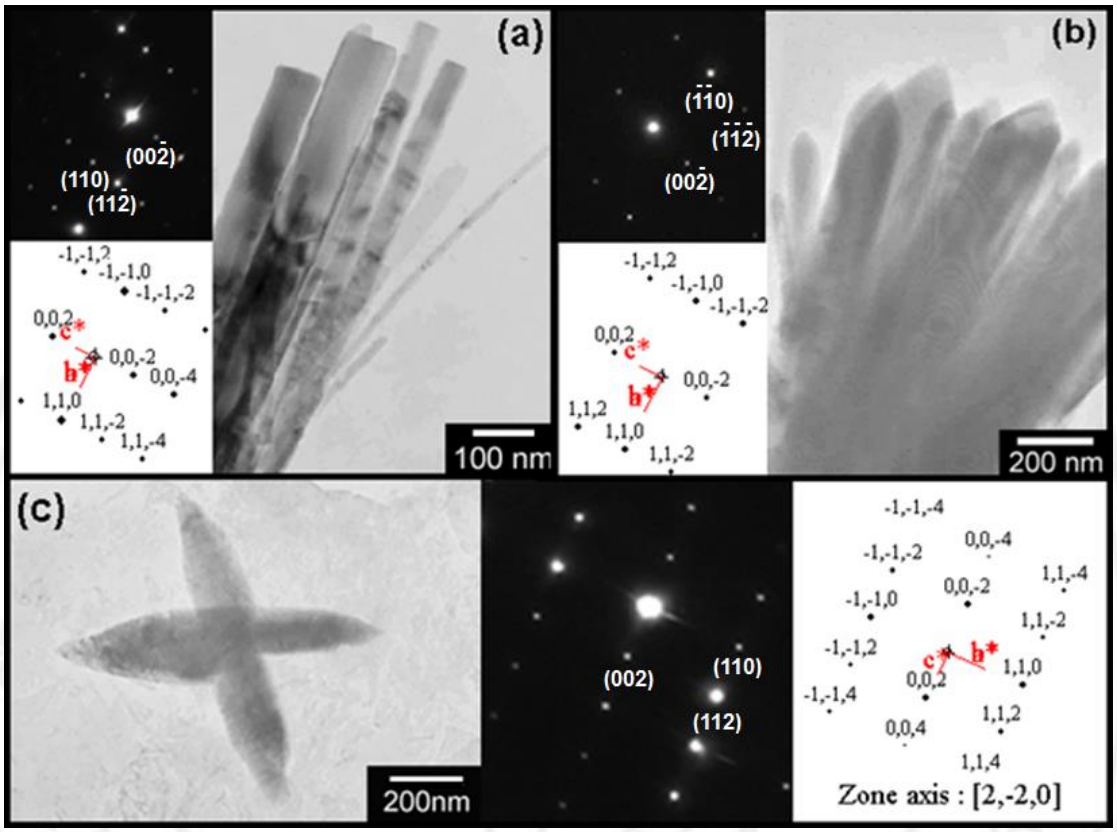

Figure 3.17 TEM images, SAED patterns and simulated patterns of ZnO synthesized in (a) NaOH, (b) LiOH and (c) NH_4OH alkaline precursor solutions.

The phase and morphologies of the ZnO products (Fig. 3.17) were further characterized using TEM and SAED. TEM images show that the rod-like, pencil-like and star-like ZnO particles were synthesized in the solutions containing NaOH, LiOH and NH_4OH as OH^- source, respectively - in accordance with the results characterized by SEM. Their corresponding SAED and simulation patterns show spot patterns which were specified as nanostructures of pure phase hexagonal wurtzite structured ZnO single crystal, in good accordance with the above XRD analysis for the phase. These patterns can be identified as the zone axis projection of electron beam on the rod-like, pencil-like and star-like ZnO [2-20]. The corresponding simulated patterns [68] with lattice vectors (a*, b* and c*) in the [100], [010] and [001] directions are in systematic arrays, and in good accordance with the results obtained by the interpretation.

5) Formation mechanism of ZnO

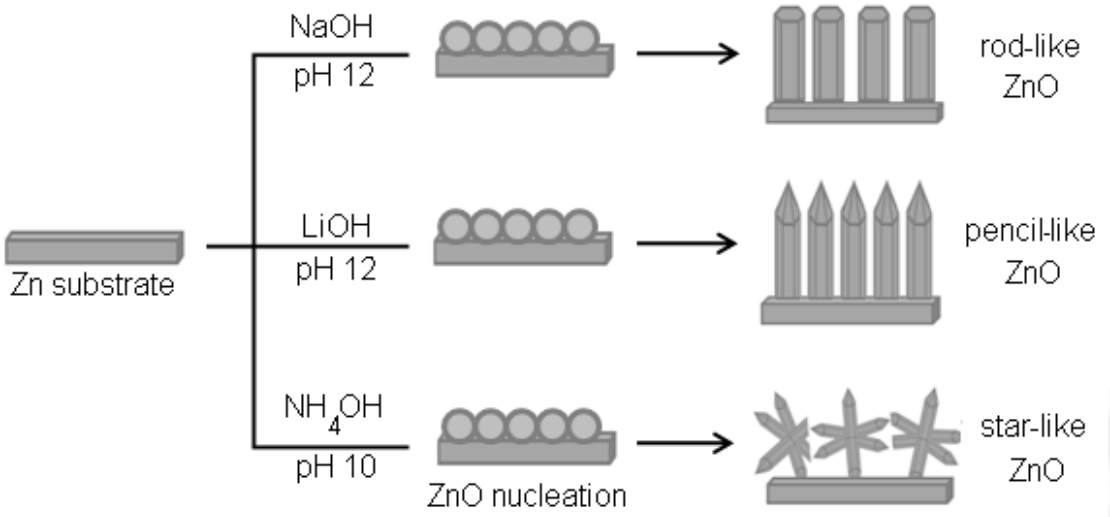

Figure 3.18 A schematic diagram for formation mechanisms of rod-like, pencil-like and star-like ZnO products.

In this research, growth of ZnO nanostructures follows the typical self-assembly process which undergoes two-step growth: nucleation and ripening states of ZnO nuclei [69]. The growth of ZnO nanostructures on Zn substrates was investigated. Oxygen in air and in the solution has the ability to oxidize zinc substrate to Zn^{2+} [70]. In NaOH and LiOH alkaline solutions, $Zn(OH)_4^{2-}$ formed. But in NH_4OH alkaline solution, additional $Zn(NH_3)_4^{2+}$ complex ions formed. $Zn(OH)_4^{2-}$ is more stable than $Zn(NH_3)_4^{2+}$ and formed by transforming of $Zn(NH_3)_4^{2+}$ [70]. During the 120 ^oC and 24 h hydrothermal reaction in alkaline solutions, $Zn(OH)_4^{2-}$ precipitated as ZnO nuclei and grew on Zn substrates with different morphologies controlled by Na^+, Li^+ and $(NH_4)^+$ cations containing in the solutions. ZnO could also be synthesized by the dehydration of $Zn(OH)_4^{2-}$ [27, 71] remaining in the precipitates.

$$Zn^{2+} + 4OH^- \rightarrow Zn(OH)_4^{2-} \quad (1)$$

$$Zn^{2+} + 4NH_3 \rightarrow [Zn(NH_3)_4]^{2+} \quad (2)$$

$$Zn(NH_3)_4^{2+} + 4OH^- \rightarrow Zn(OH)_4^{2-} + 4NH_3 \quad (3)$$

$$Zn(OH)_4^{2-} \rightarrow ZnO + H_2O + 2OH^- \quad (4)$$

Different morphologies of ZnO were synthesized due to the alkaline solution effect. It is a well-known fact that different alkaline solutions play different role in directing the reaction and crystallization of nanostructures. During hydrothermal processing, a variety of alkali dramatically influenced the precipitation, crystallization, crystal growth and morphology formation [30]. Additionally, the enclosing faces of a crystal are usually those with the lowest growth rate (the lowest surface energy). The surface energy is strongly affected by foreign ions adsorbed to the crystal surfaces [72]. Different cations of different alkaline solutions have the influence on morphology of ZnO products which developed from nanoparticles into different nanostructures (rods-like, pencil-like and star-like). A schematic diagram of the proposed formation mechanism of ZnO nanostructures is shown in Fig 3.18.

6) Photoluminescent (PL) Spectroscopy

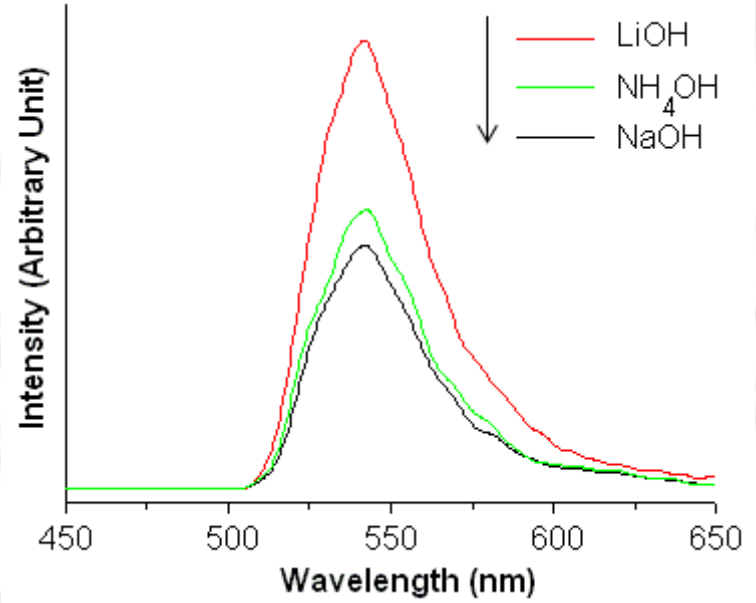

Figure 3.19 PL spectra of ZnO synthesized in NaOH, LiOH and NH_4OH alkaline precursor solutions.

The room-temperature PL spectra (Fig. 3.19) of the three ZnO nanostructured films were determined using an excitation wavelength of 215 nm. The green-yellow emission at 540 nm can be detected for all products, in accordance with those previously

reported. The emission band was attributed to the radiative recombination of photogenerated holes with electrons belonging to singly ionized vacancies on the surfaces and subsurfaces. These results suggested that the emission originates from deep level (DL) defect emission associated with oxygen vacancies of ZnO lattices, related to the structured defects [60-64,73].

7) Antibacterial Activity

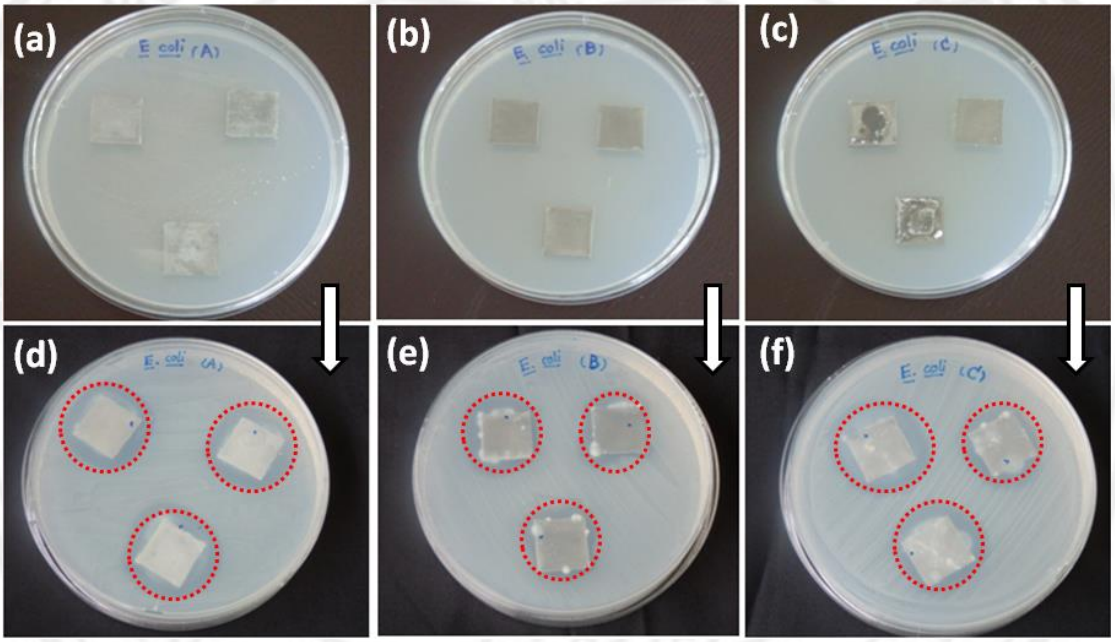

Figure 3.20 Effect of E. Coli in activation for ZnO synthesized in different alkaline precursor solutions: (a, d) LiOH, (b, e) NaOH and (c, f) NH_4OH; (a-c) before and (d-f) after incubation.

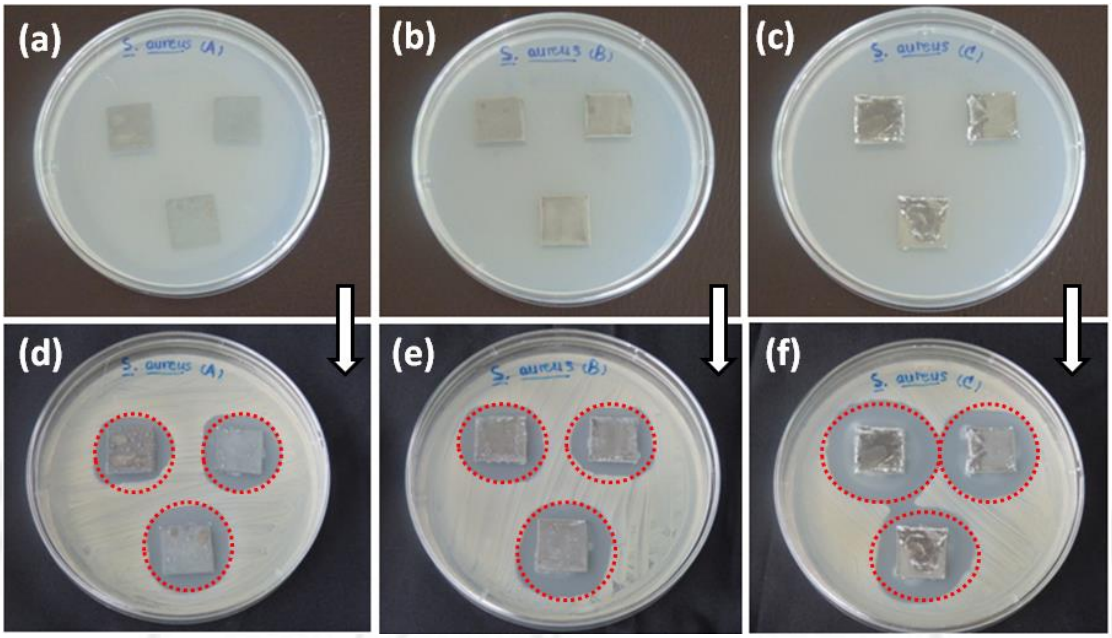

Figure 3.21 Effect of S. aureus in activation for ZnO synthesized in different alkaline precursor solutions: (a, d) LiOH, (b, e) NaOH and (c, f) NH_4OH; (a-c) before and (d-f) after incubation.

The application of the as-synthesized nanostructured ZnO films was investigated in term of qualitative antibacterial activity by applying the Kirbey-Bauer method [73]. The bactericidal activity was determined based on an inhibition zone. The photographs of Fig. 3.20 and 3.21 show the bactericidal activity of the Escherichia coli and Staphylococcus aureus, respectively. Clearly, ZnO could be used as antibactericidal agent on both of gram negative (Escherichia coli) and gram positive (Staphylococcus aureus). ZnO with different nanostructures have different physical and chemical properties on the bactericidal effect (Fig. 3.20 and Fig. 3.21). Zn ions were assumed to have minor influence on the antibacterial activity. The majority responsible for the bactericidal effect was ZnO [74]. The antibacterial activity of ZnO is considered to model the role of reactive oxygen species (ROS) generated on the surfaces [73] such as the generation of hydrogen peroxide (H_2O_2) [75,76]. Since ZnO with defects could be activated by UV light to create electron-hole (e^--h^+) pairs. The holes split H_2O molecules on ZnO particles into $OH^\bullet$ and H^+. Electrons reacted with oxygen molecules and further reacted with hydrogen ions to produce molecules of H_2O_2 [75,76]. The mechanism of light induced generation of ROS could be given as follows [76].

$$ZnO + h\nu \rightarrow ZnO + e^- + h^+ \quad (5)$$

$$h^+ + H_2O \rightarrow OH^\bullet + H^+ \quad (6)$$

$$e^- + O_2 \rightarrow {}^\bullet O_2^- \quad (7)$$

$${}^\bullet O_2^- + H^+ \rightarrow HO_2^\bullet \quad (8)$$

$$HO_2^\bullet + e^- + H^+ \rightarrow H_2O_2 \quad (9)$$

The generated H_2O_2 could penetrate cell membrane and caused trouble to the bacteria. The hydroxyl radicals and superoxide radicals with negatively charged particles could not penetrate into cell membrane and remained in contact with the outer surfaces of the bacteria. Due to the concentration difference, diffusion process proceeded. The cell walls were cleaved, elongated and caused trouble to the bacteria. A schematic diagram of antibacterial mechanism (Fig. 3.23) [73,75-77] is also shown.

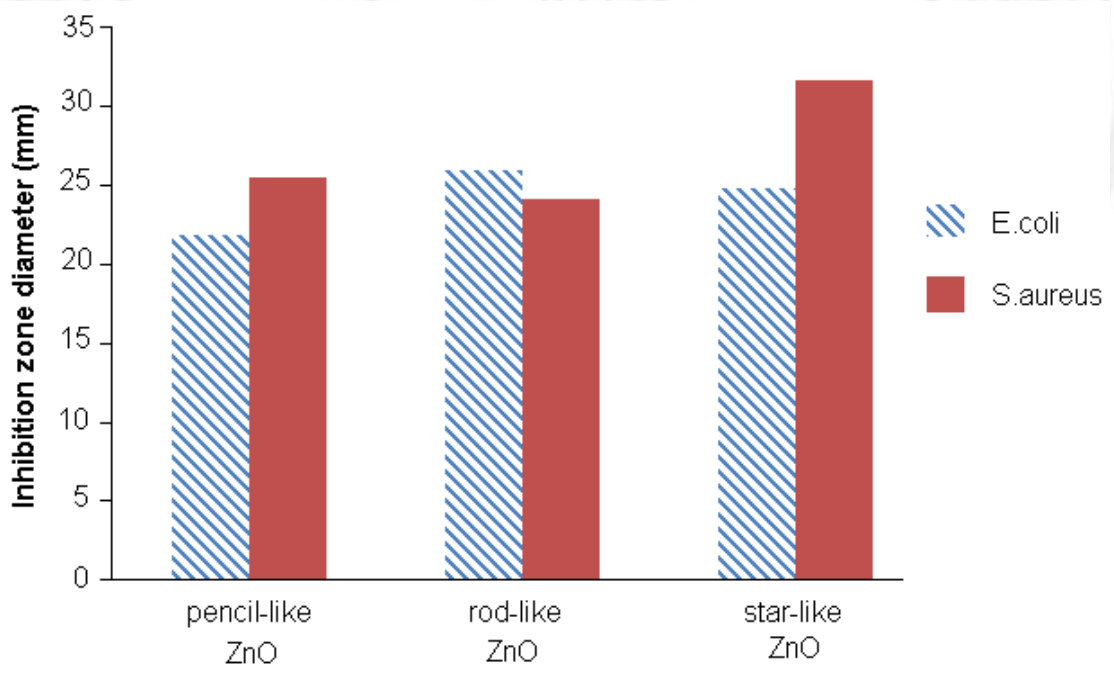

Figure 3.22 Comparative analysis of zone diameter of ZnO with different morphologies on E. Coli and S. aureus.

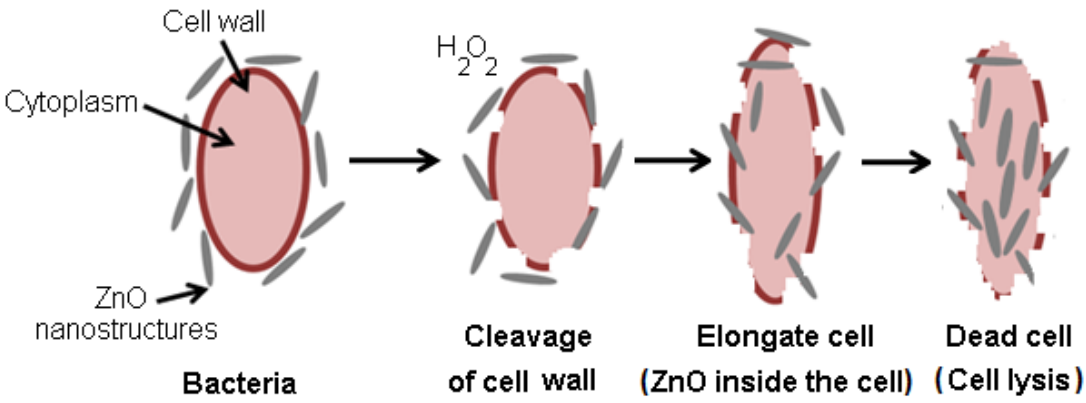

Figure 3.23 A schematic diagram of antibacterial mechanism.

3.2 Synthesis of copper oxide (CuO) by solution chemistry at room temperature

In this part, copper oxide compounds were synthesized by solution chemistry method at room temperature. CuO were fabricated on Cu metal plates as Cu source and substrate. Cu plates were cleaned with deionized water and absolute alcohol in an ultrasound bath, respectively. They were put in NaOH base solution at pH 13, kept at room temperature for 3 weeks. The final products were analyzed using XRD, SEM, TEM, and PL spectroscopy. The results and discussion are shows the morphologies, properties and the antibacterial activity of as-synthesized CuO.

1) X-ray Diffraction (XRD)

XRD patterns of CuO films grown on copper foils for different lengths of time are shown in Fig. 3.24. All of the diffraction peaks were indexed and specified as monoclinic CuO (JCPDS No. 41-0254) with lattice constants a = 4.6850 Å, b = 3.4230 Å and c = 5.1320 Å, and Cu (JCPDS No. 02-1225) [46] after 1 and 2 weeks immersion of copper foils in alkaline solution. It should be noted that the diffraction peaks of the as-synthesized CuO were strong and sharp, indicating well-crystallized products. No other impurities were detected. Upon extending the reaction time to 3 weeks, Cu_2O (JCPDS No. 05-0667) [46] was also detected. This finding is attributed to the formation of Cu_2O on the foil, caused by an incomplete reaction at the film-foil interface.

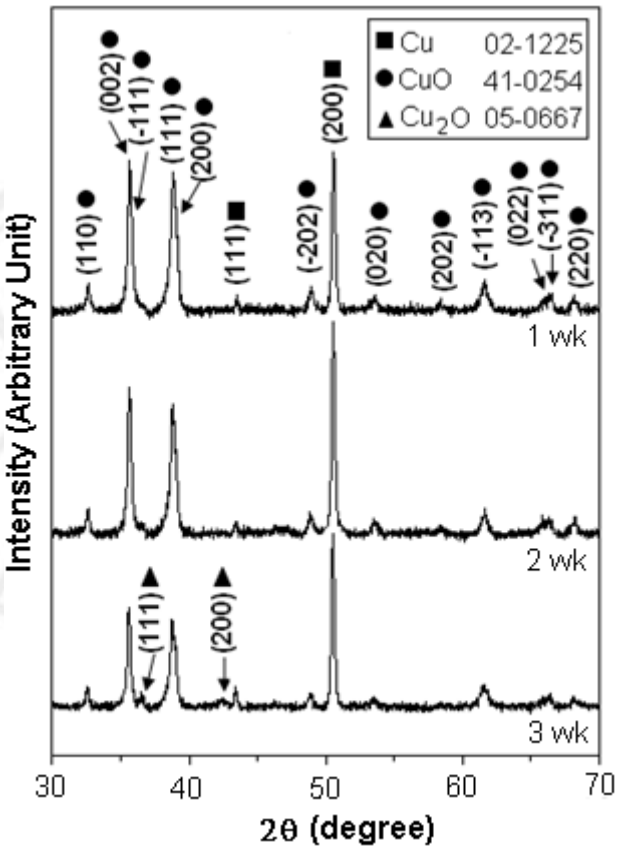

Figure 3.24 XRD patterns of CuO thin films grown on Cu foils by wet chemical method at room temperature for 1, 2 and 3 weeks.

2) Scanning Electron Microscope (SEM)

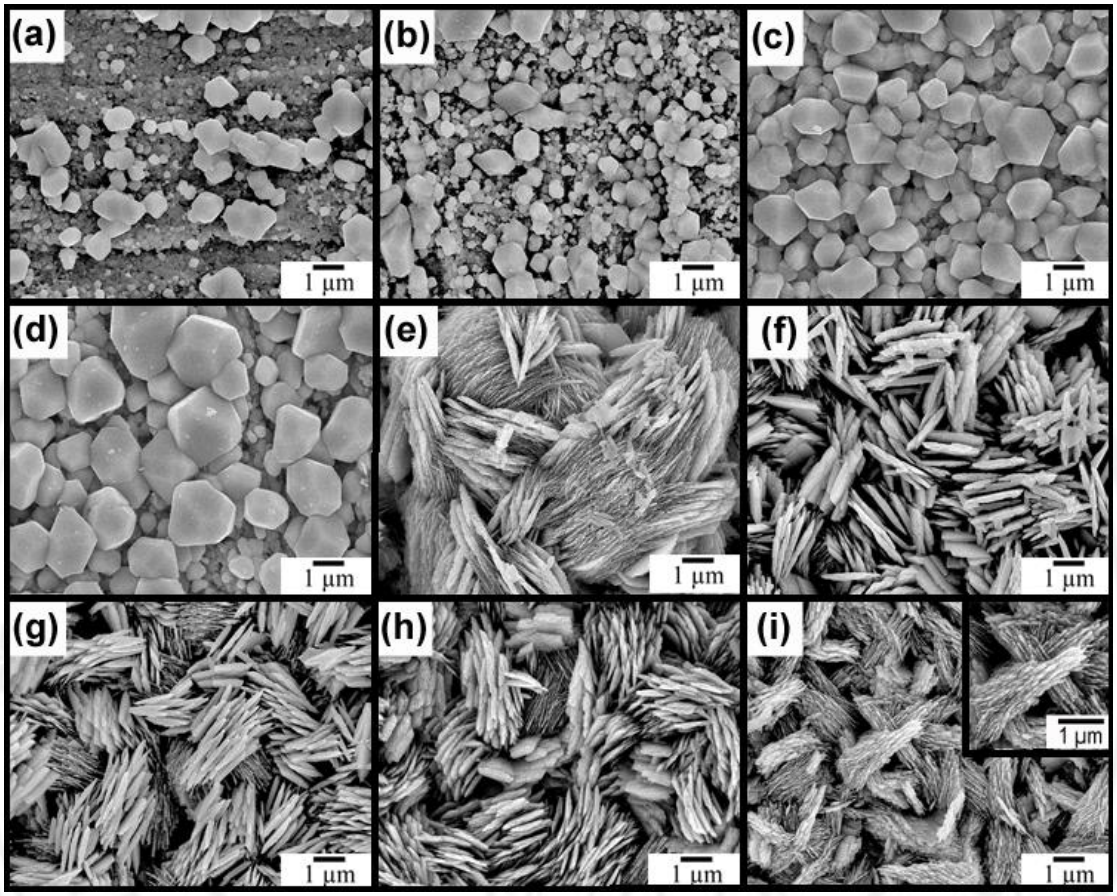

Figure 3.25 SEM images of thin films grown on Cu-foils by wet chemical method at room temperature for (a–i) 3, 5, 7, 9, 12, 14, 16, 19 and 21 days, respectively.

Morphologies and particle sizes of the films grown on Cu foils at room temperature were analyzed by scanning electron microscopy. SEM images (Fig. 3.25) show the gradual development of their morphologies and particle sizes, controlled by different lengths of reaction time and concentrations of hydroxyl ions. After 3, 5, 7 and 9 days synthesis (Fig. 3.25a–3.25d), the copper foils were covered with films consisting of a number of particles with facets and angles. Particle sizes and film thickness were increased by prolonging the synthesis time. Particles as large as 1–1.5 µm were obtained after 9 days of synthesis. The films (Fig. 3.25e–3.25i) were covered with assemblies of nanospindles with different orientations after synthesis for 12 days or longer. The sudden change of external surface morphologies from faceted and angled particles (Fig.

3.25a–3.25d) to assemblies of nanospindles (Fig. 3.25e–3.25i) was influenced by a decrease in the concentration of hydroxyl ions in the solutions (alkalinity effect), allowing nanospindles to form on top of the precursor particles. After 3 weeks synthesis, the external surface was covered with assemblies of nanospindles 1 μm wide and 2–3 μm long.

3) Transmission Electron Microscope (TEM)

To further study the morphology and crystal structure of CuO thin film, an assembly of nanospindles was analyzed by TEM. Fig. 3.26a shows an assembly of nanospindles synthesized at room temperature for 2 weeks. The SAED pattern (Fig. 3.26b) indicated pure monoclinic CuO single crystal with [00-1] as the zone axis, which was in good accordance with XRD analysis. The simulated pattern [68] (Fig. 3.26c) with a*, b* and c* reciprocal lattice vectors in the [100], [010] and [001] directions was in a systematic array, and in good accordance with that obtained by the interpretation. The crystal structure of monoclinic phase CuO was simulated using the atomic positions of Cu (0.25, 0.25, 0) and O (0, 0.5789, 0.25) [78], as shown in Fig. 3.26d. It belongs to the monoclinic crystal system, with C2/c space group. The copper atom is coordinated by 4 oxygen atoms in an approximately square planar configuration [78].

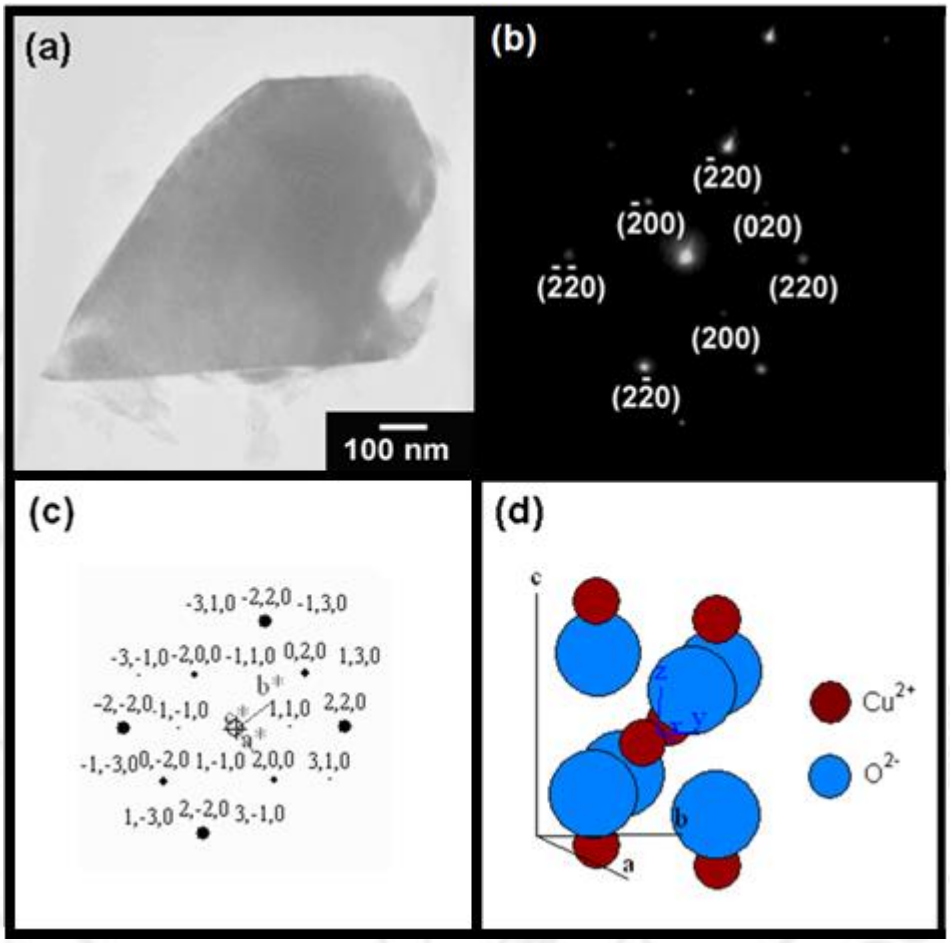

Figure 3.26 (a) TEM image and (b) SAED pattern of an assembly of nanospindles grown on copper foil by wet chemical method at room temperature for 2 weeks. (c, d) The simulated pattern and unit cell of a spindle.

4) Formation mechanism of CuO

During the initial stage of synthesis, clean and fresh copper foils were separately immersed in 10 ml NaOH solutions at room temperature. Cu foils (copper sources) dissolved in the solutions as Cu^{2+} ions with electrons left behind. The oxidation rate was very fast, and the Cu^{2+} ions were continuously released into the solutions [79]. The released ions combined with hydroxyl ions to form $Cu(OH)_2$ precipitates (ppts) on top of the copper foils, which were transformed into CuO (solid films) after 12 h dehydration at 70°C, in accordance with the most stable oxidation states of copper (2+) and oxygen (2–). At high OH^- concentration, $[Cu(OH)_4]^{2-}$ complex ions could also form, which precipitated as $Cu(OH)_2$ and decomposed into CuO (solid films) by the dehydration process. Possibly, dissolved O_2 in the alkaline solutions directly accepted the electrons, forming CuO (ppts). At this stage, the concentration of OH^- ions influences the nucleation and growth processes, such as the content of nuclei and growth units [80] and the growth rate of different crystalline faces, thus leading to the formation of anisotropic particles [81].

$$Cu^0 \rightarrow Cu^{2+} + 2e^-$$
$$Cu^{2+} + 2OH^- \rightarrow Cu(OH)_2 \text{ (ppts)}$$
$$Cu(OH)_2 + 2OH^- \rightarrow [Cu(OH)_4]^{2-} \text{ (complex ions)}$$
$$2[Cu(OH)_4]^{2-} \rightarrow 2Cu(OH)_2 \text{ (ppt)} + 2H_2O + O_2 + 4e^-$$
$$Cu(OH)_2 \rightarrow CuO \text{ (solid films)} + H_2O$$
$$O_2 \text{ (dissolving oxygen in solutions)} + 4e^- \rightarrow 2O^{2-}$$
$$Cu^{2+} + O^{2-} \rightarrow CuO \text{ (ppts)}$$

After a sufficient length of time, the oxidation rate slowed down; this was controlled by the diffusion rate of oxygen ions through the $Cu(OH)_2$ solid films coated on the copper foils. Ultimately, oxygen ions diffused through the $Cu(OH)_2$ films to the film-foil interfaces due to the concentration gradient. However, there was a deficiency of oxygen ions at the film-foil interfaces. Thus, the incomplete reaction process (due to deficient oxygen and rich copper) resulted in the formation of Cu_2O (solid) coating on the copper foils, in accordance with the oxidation states of copper (1+) and oxygen (2–).

$$Cu^{0} \rightarrow Cu^{1+} + e^{-}$$

$$2Cu^{1+} + O^{2-} \rightarrow Cu_2O \text{ (solid)}$$

The formation of solid films on copper foils is schematically shown in Fig. 3.27

.

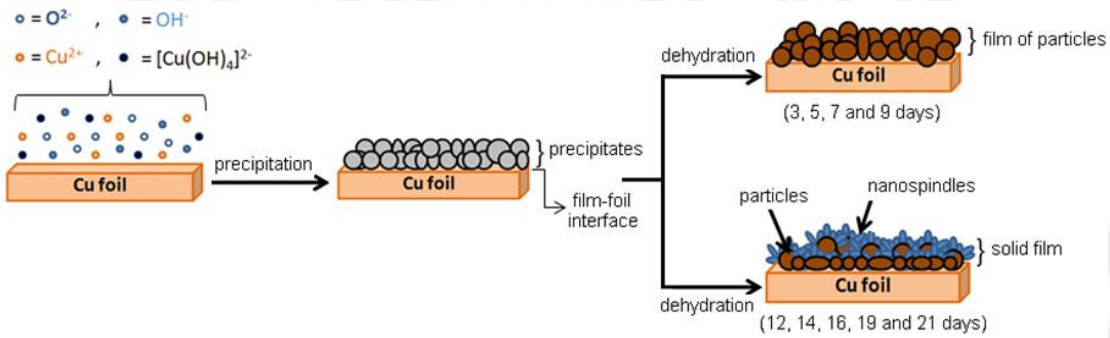

Figure 3.27 Different stages for the formation of solid thin films on copper foils.

5) Photoluminescent (PL) Spectroscopy

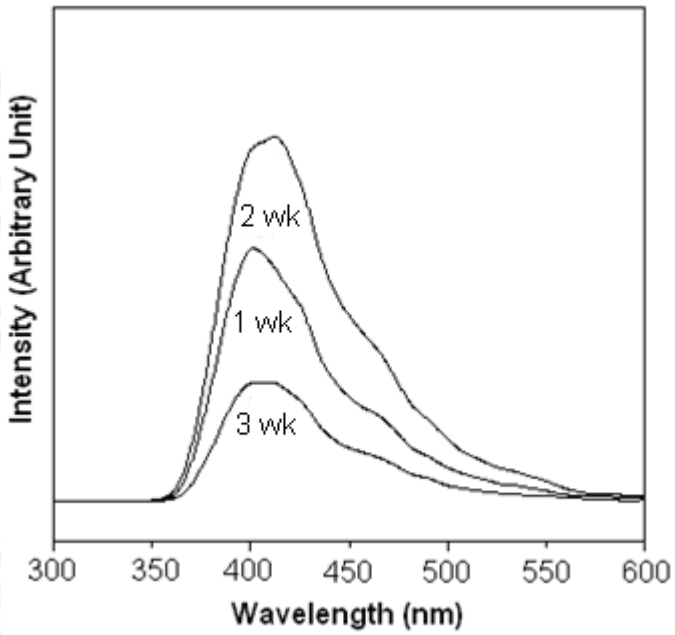

Figure 3.28 PL spectra of thin films grown on Cu foils by wet chemical reactions at room temperature for 1, 2 and 3 weeks.

Photoluminescence (PL) spectroscopy was used to study the emission properties of the products (Fig. 3.28). The electronic transition between the higher sub-levels of the conduction band and the Cu d-shell of the valence band [82] led to three PL emissions after different lengths of reaction time. Emissions from CuO thin films synthesized for 1 and 2 weeks, respectively, appeared as violet luminescent bands at 400 nm (3.10 eV) and 413 nm (3.00 eV) with broad tails in the green spectral region [83]. Upon increasing the reaction time from 1 to 2 weeks, the PL intensity strengthened. However after 3 weeks synthesis, the PL intensity was the lowest. The mixed phases of CuO and Cu_2O likely formed some undesired defects in the product, leading to the broadened and lowered peak.

6) Antibacterial Activity

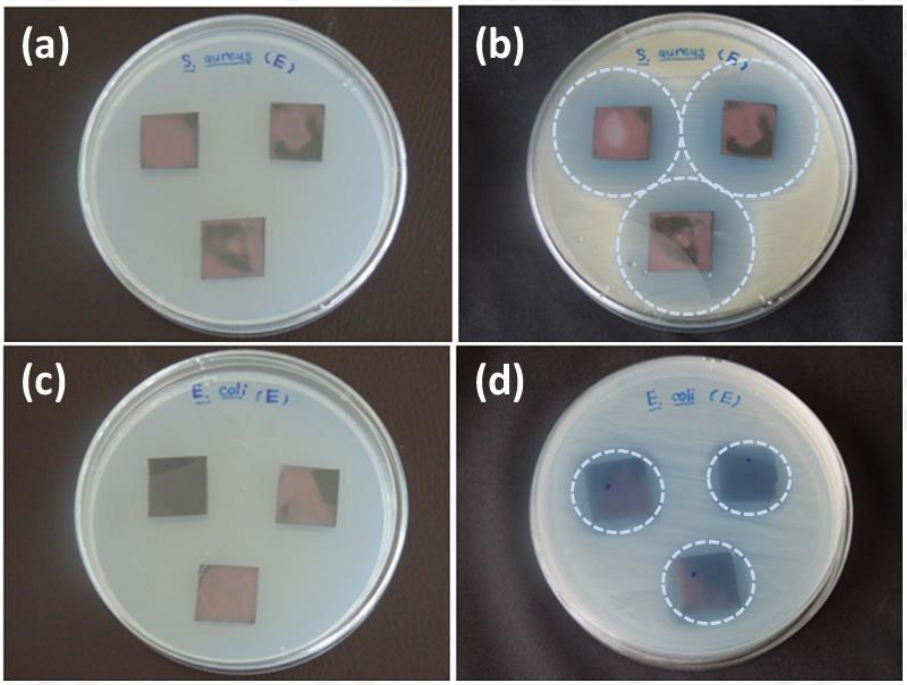

Figure 3.29 Antibacterial activity of CuO thin films for (a, b) S. aureus, and (c, d) E. coli. (a, c) before and (b, d) after testing.

In this research, CuO thin film synthesized for 2 weeks was determined to be optimal for studying antimicrobial activity. CuO thin film demonstrated antimicrobial activities against *Gram-positive (S. aureus)* and *Gram-negative (E. coli)* bacteria strains. The antimicrobial activities of CuO thin film were studied using the modified Kirby-Bauer method by observing an inhibition zone around the thin film [73]. In these tests, CuO thin films on Cu foils partially covered the NB agar disk. Bacteria with 0.3 OD were then sprayed on top. After 24 h incubation, bacterial growth in the NB agar was visualized (Fig. 3.29); diameters of the inhibition zones around the CuO thin films were measured as 25.17 mm for *S. aureus* and 22.50 mm for *E. coli*. Their different sensitivities appear to be related to the nature of their cell wall structures. *S. aureus* is composed of multiple layers of peptidoglycan with numerous pores that were more susceptible to the intracellular transduction caused by the CuO thin film, leading to cell wall disruption. In contrast, the cell walls of *E. coli* are relatively thin, mainly consisting of peptidoglycan and outer layers of lipopolysaccharide, lipoprotein and phospholipids, which would be less prone to be attacked by the CuO thin film [84]. In summary, CuO thin film has higher antibacterial activity against *S. aureus* than *E. coli*.

Copper is a structural constituent of enzymes in many living microorganisms. Furthermore, free Cu^{2+} ions at high concentrations are able to produce hazardous effects by generating reactive oxygen species (ROS) such as $\bullet O_2^-$, $\bullet HO_2$, $\bullet OH$ and H_2O_2 [32], which cause serious disruptions to amino acid synthesis and DNA [23]. The production of ROS by CuO in the environment of modified agar diffusion assays was achieved by the following sequence. O_2 molecules were reduced by photogenerated electrons to form $\bullet O_2^-$ superoxide anion radicals [32]. At the same time, H_2O molecules were decomposed into H^+ and OH^- by photogenerated holes [85]. The $\bullet O_2^-$ superoxide anion radicals reacted with H^+ to generate $\bullet HO_2$ radicals, which collided with electrons to produce HO_2^- hydrogen peroxide anions. The HO_2^- hydrogen peroxide anions reacted with hydrogen ions to produce H_2O_2 molecules [23]. $\bullet OH$ radicals could be synthesized by the collision of photogenerated holes and H_2O molecules [86]. In the end, the generated ROS initially interacted with outer cell walls and further generated free radicals. The radicals penetrated the inner cell membranes which led to serious disruption of their internal contents; the cells became deformed and disorganized,

causing leakage [32]. When the combination processes was not possible, electron-hole pairs could be recombined together to generate heat inside the CuO thin film. In summary, CuO thin film demonstrated excellent antibacterial performance, killing the bacteria by generating ROS to disrupt them.